

CHAPTER 2. LITERATURE REVIEW AND THEORETICAL BACKGROUND

2.1. Bedforms

Much research has been done in the past on the mechanics and prediction of bedforms. The physical processes underlying bedform mechanics is complex. Karim (1999) lists among the factors leading to this complexity as 1) a large number of governing variables and their interaction; 2) the 3-dimensional nature of bedforms and their development; 3) lags in the development of bedform adjustment in response to changes in the structure of the flow; and 4) problems with measuring bedform dimensions in the field. Among the earliest analytic treatments of bedforms is that of DuBuat (1786) as mentioned by Graf (1971). DuBuat described the bedform as being triangular in shape and slowly advancing. The bedform advancement was caused by the individual grains moving up the gentle slope, arriving at the summit only to fall rapidly down the steep slope, and finally being sheltered from the flow in the trough between successive bedforms.

An extensive set of laboratory studies of bedforms were conducted and compiled by the U.S. Geological Survey at Colorado State University in the 1950's and 1960's. These data, summarized in Guy and others (1966), are the impetus for a classification system for bedforms developed by Simons and others (1965A) and presented as table 2.1, with each type of bedform illustrated in figure 2.1. Simons and others (1961) also suggested classifying the bedforms using the Froude number (Fr) (equation 1.9) However, it was recognized that this was not an absolute classification but rather qualitative as Simons and others point out that a particular bedform occurred in the laboratory flume at $Fr < 0.6$

but in a large deep river at $Fr < 0.3$. This result possibly is indicative of the variable nature of the Froude number across a stream and the contrast between local Froude number with reach-averaged Froude number, along with scale effects.

| Flow regime | Bedform | Bed material concentrations, ppm | Mode of sediment transport | Type of roughness | Roughness, $\frac{C}{\sqrt{g}}$ |
|--------------|------------------|----------------------------------|----------------------------|------------------------------|---------------------------------|
| Lower regime | Ripples | 10-200 | Discrete steps | Form roughness predominates | 7.8-12.4 |
| | Ripples on dunes | 100-1,200 | | | -- |
| | Dunes | 200-2,000 | | | 7.0-13.2 |
| Transition | Washed-out dunes | 1,000-3,000 | | Variable | 7.0-20.0 |
| Upper regime | Plane beds | 2,000-6,000 | Continuous | Grain roughness predominates | 16.3-20 |
| | Antidunes | 2,000→ | | | 10.8-20 |
| | Chutes and pools | 2,000→ | | | 9.4-10.7 |

Table 2.1—Classification of bedforms and other information (adapted from Graf, 1971)

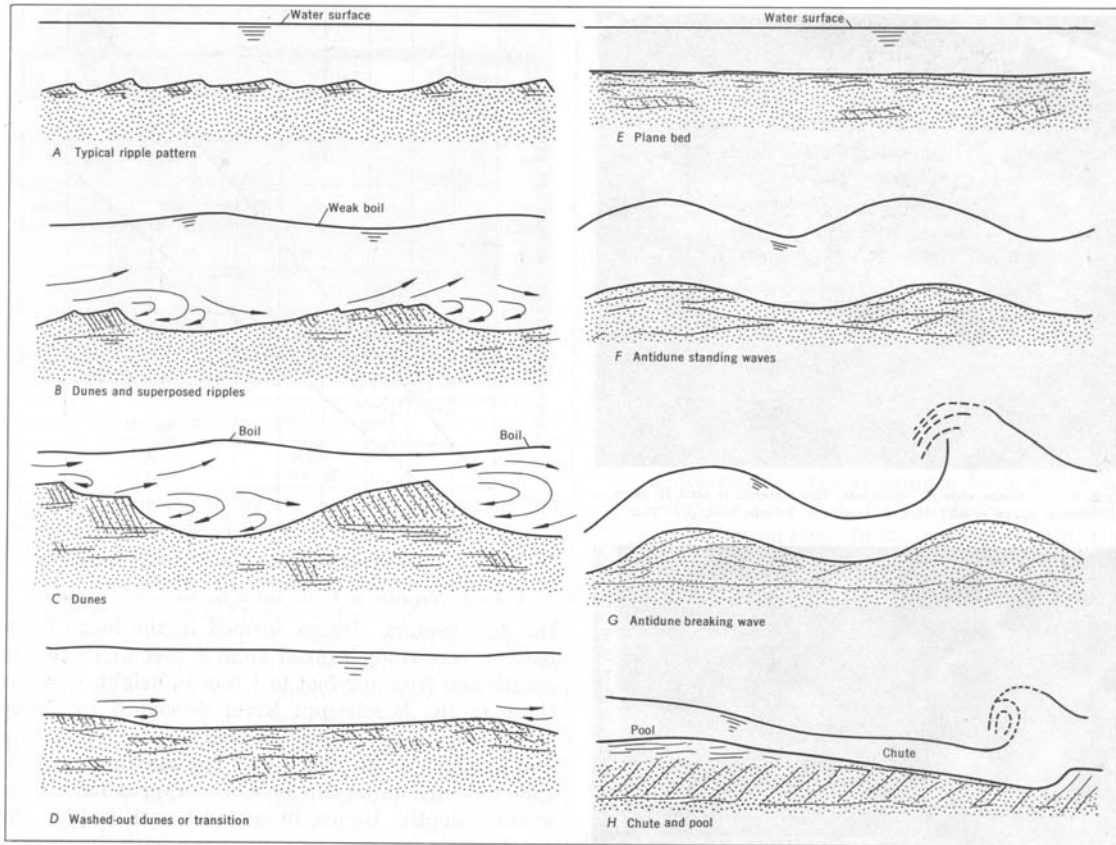


Figure 2.1.—Forms of bed roughness in an alluvial channel (from Simons and Richardson, 1966)

The American Society of Civil Engineers (ASCE) (1966) summary report from the task force on bedforms provides descriptions and definitions of the various types of bedforms. Vanoni (1975) presented a table that contained the more salient points of the ASCE task force report and is reproduced as table 2.2. This table is similar to that produced by Simons and others (1961).

| Bed form or configuration (1) | Dimensions (2) | Shape (3) | Behavior and occurrence (4) |
|-------------------------------|---|--|--|
| Ripples | Wavelength less than approx 1 ft; height less than approx 0.1 ft. | Roughly triangular in profile, with gentle, slightly convex upstream slopes and downstream slopes nearly equal to the angle of repose. Generally short-crested and three-dimensional | Move downstream with velocity much less than that of the flow. Generally do not occur in sediments coarser than about 0.6 mm |
| Bars | Lengths comparable to the channel width. Height comparable to mean flow depth | Profile similar to ripples. Plan form variable | Four types of bars are distinguished: (1) Point; (2) alternating; (3) Transverse; and (4) Tributary. Ripples may occur on upstream slopes |
| Dunes | Wavelength and height greater than ripples but less than bars | Similar to ripples | Upstream slopes of dunes may be covered with ripples. Dunes migrate downstream in manner similar to ripples |
| Transition | Vary widely | Vary widely | A configuration consisting of a heterogeneous array of bed forms, primarily low-amplitude ripples and dunes interspersed with flat regions |
| Flat bed | — | — | A bed surface devoid of bed forms. May not occur for some ranges of depth and sand size |
| Antidunes | Wave length = $2\pi V^2/g$ (approx) ^a Height depends on depth and velocity of flow | Nearly sinusoidal in profile. Crest length comparable to wavelength | In phase with and strongly interact with gravity water-surface waves. May move upstream, downstream, or remain stationary, depending on properties of flow and sediment. |

^a Reported by Kennedy (1969).

Table 2.2—Summary description of bedforms and configurations (from Vanoni, 1975 and ASCE, 1966)

Lower-flow and transitional-flow regimes are of interest in this study as the large alluvial rivers of interest in this study are wide with low Froude (Fr) numbers and the bedforms of interest have lengths that scale with the flow depth. Thus, flat bed, ripples, and dunes

will be the primary bedforms present and of interest. Furthermore, as van Rijn (1984C) states, low flow and transitional flow regimes are the most important for field conditions. Yalin and da Silva (2001) characterize those large-scale bedforms, where lengths scale with the flow depth as dunes, whereas those bedforms whose lengths are proportional to flow width are termed bars.

Ripples and dunes are skewed in shape (in side view) and flow over them produces eddies in their lees (Haque and Mahmood, 1985). Exner (1925) provided the first modern analysis of bedforms by using perturbation stability theory on the equations of fluid motion, fluid continuity, and sediment continuity, including a sediment-transport relation for closure (Kennedy and Odgaard, 1991). This analysis demonstrated how a symmetric bedform evolves into a non-symmetrical, skewed feature as often found on the bed of rivers. Ripples and dunes have different geometric scales, with the ripple height being smaller than that of dunes and substantially smaller and independent of the flow depth. Ripple length is dependent on sediment size and independent of the flow depth (Engelund and Fredsoe, 1982). The dune height is highly dependent on the flow depth and the dune length is much larger than (but proportional to) the flow depth (van Rijn, 1984C).

Whereas dunes and ripples are different in the above-mentioned ways, their geometries are similar (Haque and Mahmood, 1985). Both dunes and ripples have a gentle, slightly convex-to-the-flow, slope to the stoss (upstream) face, with a downstream face that is steep and slightly less than the angle of repose of the sand (see figure 2.2)

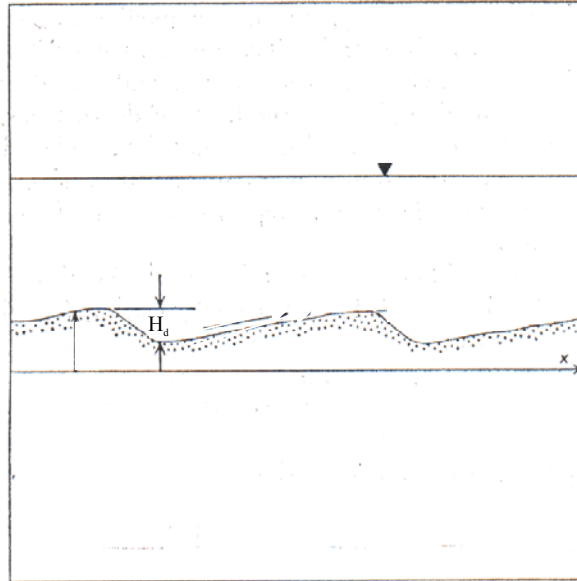


Figure 2.2.—Conceptual drawing of dunes (from Simons and others, 1965)

Kennedy and Odgaard (1991) provide an excellent review of some of the principal bedform studies since 1925 and group the studies into three categories: 1) analytical models (predominantly of stability theory) (Exner, 1925; Anderson, 1953; Kennedy, 1963; Kennedy, 1969; Hayashi, 1970; Engelund, 1970; Gill, 1971; Fredsoe, 1974; Richards, 1980; Fredsoe, 1982; and Haque and Mahmood, 1985), 2) empirical relations (Garde and Anderson, 1959; Yalin, 1964; Ranga Raju and Soni, 1976; Yalin and Karahan, 1979; Jaeggi, 1984; Ikeda, 1984; van Rijn, 1984C; and Menduni and Paris, 1986), and 3) statistical analysis (Nordin and Algert, 1966; Hino, 1968; Annambhotla, Sayre and Livesay, 1972; and Jain and Kennedy, 1974). The main issues of interest in this review are: 1) origin of bedforms and 2) predicting their type and geometry. As such, this review is divided accordingly, with a sub-grouping similar to that of Kennedy and Odgaard (1991) when prediction of geometry is discussed.

2.1.1 Origin of Bedforms

As discussed previously, various bedforms have been associated with various flow regimes. A typical progression of bedforms for a sand-bed stream was listed by Garcia (1999) as follows:

“The bed is assumed to be initially flat. At low imposed velocity U , the bed remains flat because no sediment is moved. As the velocity exceeds the critical value, ripples are formed first. At higher values, dunes form and coexist with ripples. For even higher velocities, well-developed dunes form in the absence of ripples.

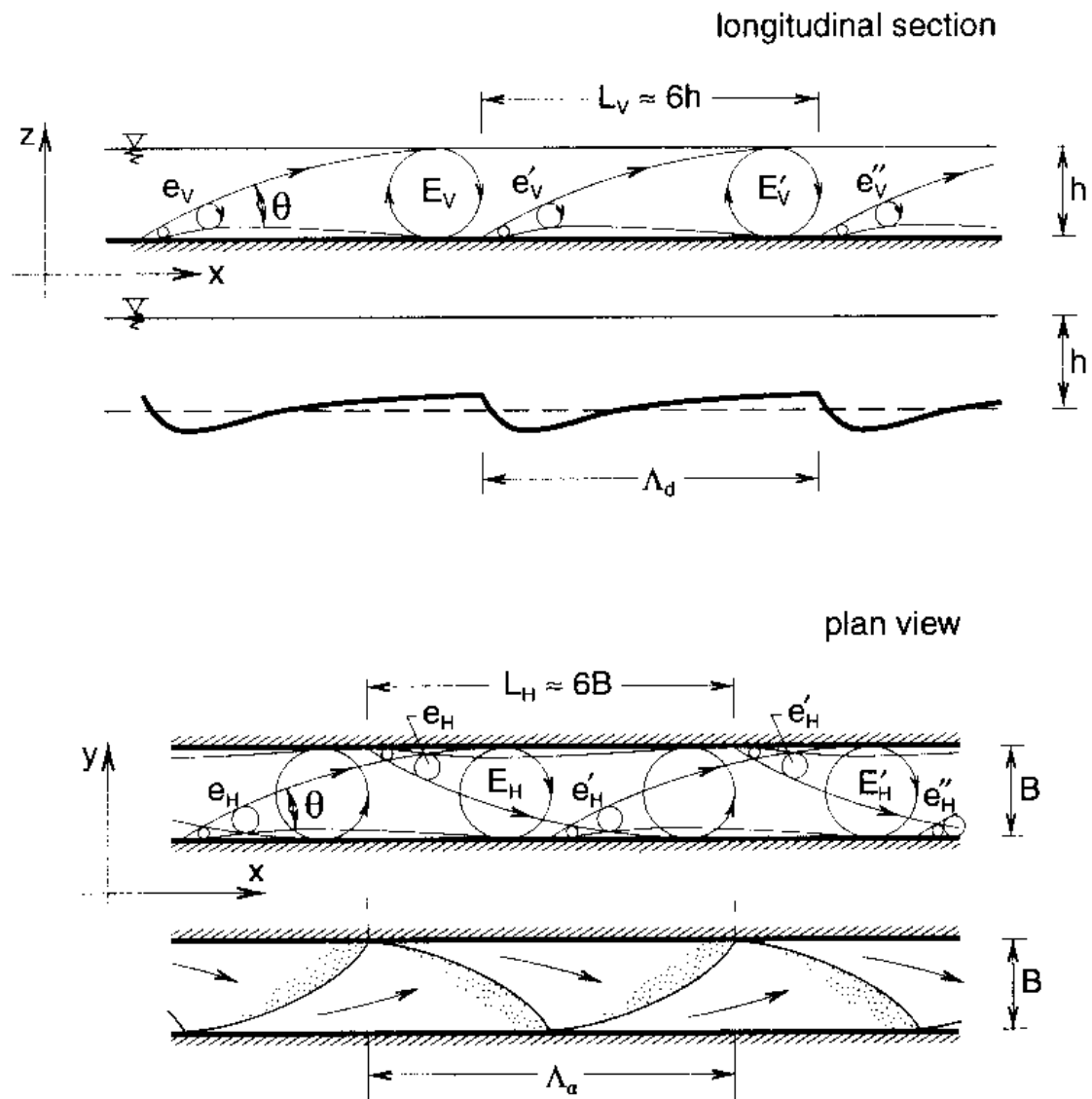
At some point, the velocity reaches a value near the critical value in the Froude sense. Near this point, the dunes often are suddenly and dramatically washed out. This results in a flat bed known as an upper-regime (supercritical) flat bed.
.....

In the case of a bed coarser than 0.5 mm, the ripple regime is replaced by a zone characterized by a lower-regime (subcritical) flat bed. Above this lie the ranges for dunes, the upper-regime flat bed, and antidunes.”

Until recent experiments by Coleman and Eling (2000) showed that bedforms could develop in laminar flow, theories developed for bedforms were thought to apply for fully

turbulent flow (Yalin, 1977A). According to Yalin and da Silva (2001), citing work of Matthes (1947), Velikanov (1955), Kondratiev and others (1959) and Grishanin (1979), many prominent researchers have long maintained that large-scale bedforms (dunes) are caused by large-scale turbulence. Kennedy and Odgaard (1991) cite that the instability that produces ripples and dunes is similar to that which causes turbulence and that any disturbance rapidly amplifies to the extent that equilibrium turbulence or bedforms soon emerge. Internal non-uniformities of the flow, caused by turbulent bursts, result in the initially flat mobile bed transforming into a bed covered with dunes (Yalin and da Silva, 2001). These bursting processes from a deterministic sense are described in figure 2.3 (Yalin and da Silva, 2001, p. 26) (in other words, the process as shown in the figure has the random element which is typical of turbulence removed for ease of illustration). The bursting process is the evolution of large macroturbulent eddies (Yalin and da Silva, 2001), which begin as small eddies in the areas of large shear stresses near the bed. The small eddies develop as a result of the excessive fluctuation in shear stresses. Once mobilized, these small eddies are conveyed by the flow downstream, while simultaneously moving away from the boundary, and diffusing and coalescing to become larger and fewer. These burst-forming eddies grow to scale with the flow depth and at that point they impinge on the bed, causing the large eddy to break apart, entrain sediment, and form new small eddies that then repeat the same cycle. Yalin and da Silva (2001) report that ripples are prominent when the flow is hydraulically smooth with a viscous layer near the bed. It is reported that ripple geometry is not dependent on the overall flow dimensions and, therefore, unlikely that ripples are affected by the bursting process, with the viscous region “shielding” the bed from the action of the bursts (Yalin

and da Silva, 2001). According to van Rijn (1984C), the generation of ripples appears to be dependent on the stability of the granular surface under the action of turbulent velocity fluctuations; however, this result would seem to be in contradiction to the notion of development of these ripples in a viscous (or laminar) sublayer environment.



EXPLANATION

- e_v = “burst-forming” vertical eddies
- e_H = “burst-forming” horizontal eddies
- E_v =large scale vertical eddies
- E_H =large scale horizontal eddies
- h =flow depth
- B =width
- L_v =vertical burst length
- L_H =horizontal burst length
- Λ_d =dune length
- Prime symbol designates new eddies

Figure 2.3.—Evolution of eddies (from Yalin and da Silva, 2001)

These conceptual understandings of the effects of turbulence on the formation of bedforms are now in question because of the findings of Coleman and Eling (2000). Coleman and Melville (1996) introduce the term sand wavelets (smaller than ripples) to describe the instability induced “nascent” bedforms that are precursors to the development of ripples and dunes. These sand wavelets are said to begin from random sand pileups, which also was noted in the experiments of Williams and Kemp (1971). Coleman and Melville (1994) note that the process of bedform generation from flat bed conditions is the result of sand-water interface instability (as opposed to turbulence?). Coleman and Eling (2000) note that these waves appear to not be a consequence of turbulence but rather generated by a form of shear layer instability or instability of the motion of the granular mass moving over the otherwise flat sediment bed. Ripples and dunes are the result of the same type of wavelets, with the difference in bedform dependent on different flow instability mechanisms at subsequent development stages to provide either ripples or dunes (Coleman and Melville, 1996).

In the classic analysis by Exner (detailed in Leliavsky, 1955 (see Nelson and others, 1993)), an initially symmetric incipient bedform will tend to become asymmetrical as the bedform grows and migrates. Flow separation occurs at the crest of each bedform, with a reattachment point somewhere on the stoss face of the next downstream bedform. A schematic depiction of the typical flow field over a bedform is shown in figure 1.1 (from Nelson and others, 1993). The shaded portion is the typical wake-like flow structure, however, this region also has the effect of the topographically induced acceleration of

flow and the presence of the bed. Beneath this wake region is where the internal boundary layer is growing downstream of the reattachment point.

When dunes are fully developed, regions of increased and decreased bed-shear stress are present, resulting in regions of scour and deposition. If stage continues to increase, sediment particles from the bed will go into suspension according to the ratio between the grain shear stress and the particle fall velocity. This process will result in washed-out dunes (or transition regime) (van Rijn, 1984C). The observations of Jordan (1965) and the data of Shen and others (1978) indicate that for flows with large depths, the transitional bedforms (washed out dunes) maintain their height but are longer, which is not observed in flume-scale data (Bennett, 1995). Amsler and Garcia (1997) cite that large dunes on the Parana River decreased in magnitude with increasing discharge, however, the superimposed dunes increased in size.

2.1.2 Prediction of Bedform Type and Geometry

Fully understanding bedforms and their prediction is difficult because the bedforms, and, thus, hydraulic form roughness, are dependent on flow conditions and sediment transport. In turn, these flow conditions are highly dependent on the channel-bed configuration and its form roughness (van Rijn, 1984C). Prediction of the type and dimension of bedforms are of great interest to investigators. There are numerous investigators who have proposed relations to predict the dimensions of the bedforms. The dimensions of interest are the amplitude or bedform height (H_d) and the bedform length (λ). In some of the

literature, bedform steepness is referred to as the bedform height divided by the bedform length (H_d/λ). As this research is limited to the lower regime, the discussion will be limited to that of the lower flow regime relations (dunes and ripples).

2.1.2.1 Prediction of Bedform Type

A large number of methods have been proposed to identify the bedform type. One of the earliest attempts at classification was that of Forchheimer (1930), who suggested that the Froude number (Fr) served as a good criterion to separate the occurrence of antidunes ($Fr > 1$) with the occurrence of dunes ($Fr < 1$). Most of the methods involve graphs with observed data (mostly from laboratory analysis (Raudkivi, 1990)) whereby certain classification zones are identified for various types of bedforms.

Simons and Richardson (1966) present a method, that unlike many of the other methods, which use dimensionless parameters in the graph, uses a dimensional plot of streampower (Bagnold, 1960) (product of the bed shear stress and the mean velocity) versus the median grain size (figure 2.4). Vanoni (1975) points out that whereas the data from the Rio Grande reported in Nordin (1964) agree well with the Simons and Richardson graph, the data collected by Jordan (1965) on the Mississippi River, with similar velocities but depths as much as 10 times greater than the Rio Grande, would indicate plane bed conditions on the graph when clearly dunes were present. Shen and others (1978) also report that their data from the Missouri River does not agree with this graph. This

disagreement would seem to indicate that failure to non-dimensionalize the graph has introduced scale effects into the procedure, as the graph was constructed from laboratory data and field data from the Elkhorn River near Waterloo Nebraska; Rio Grande above El Paso Texas; Middle Loup River at Dunning, Nebraska; Rio Grande at Cochiti, New Mexico; Rio Grande near Bernalillo, New Mexico; Rio Grande at Angostura, New Mexico; Punjab Canal data; and assorted canal data from Harza Engineering. All these rivers have shallower depths than that of the Mississippi and Missouri Rivers.

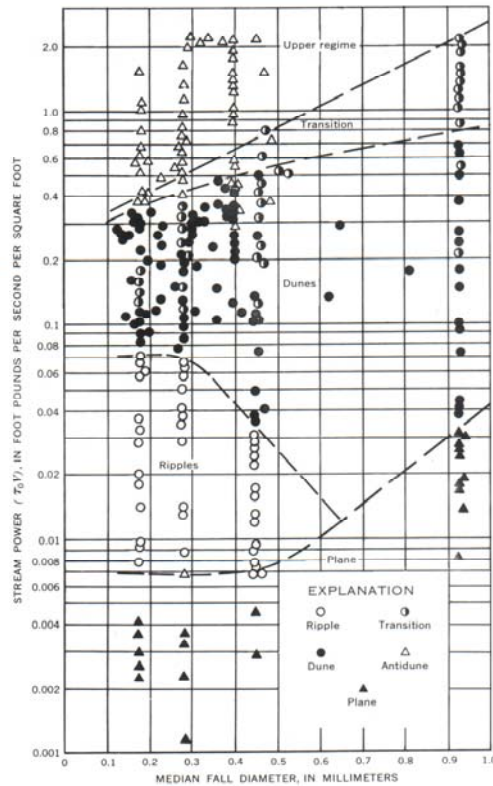
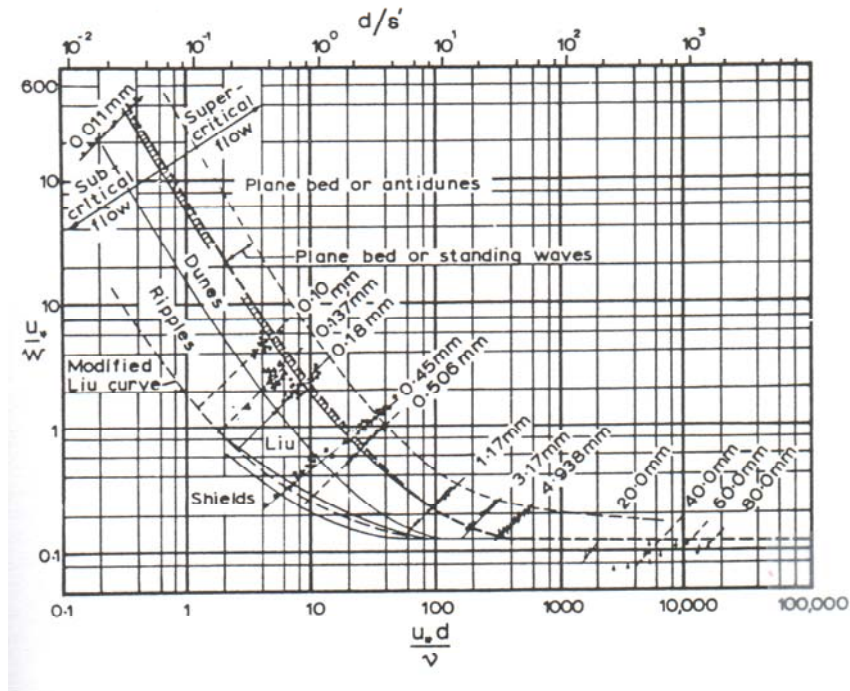


Figure 2.4.—Bedform predictor from Simons and Richardson (1966)

Liu (1957) uses dimensionless shear velocity and shear velocity Reynolds number to delineate the zones (figure 2.5). According to Simons and Senturk (1977), the diagram of

Liu (1957) does not give acceptable results for field conditions because few field data were used in the analysis.

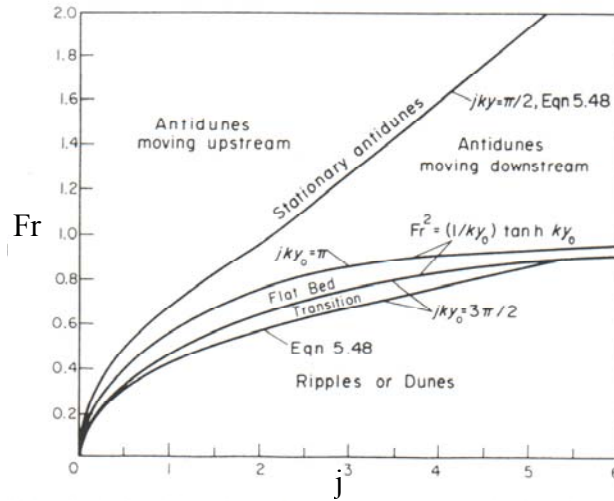


EXPLANATION

- u_{*}=shear velocity
- w=sediment particle fall velocity
- d=sediment size
- ν=kinematic viscosity

Figure 2.5.---Bedform predictor from Liu (1957)

Kennedy (1969) presents a graph (figure 2.6) based on his two-dimensional potential flow model and experimental data that characterize the bedform based on a relation between the Froude number and j , which is the ratio between the lag distance, δ , and the depth of flow, H . The lag distance is a phase shift between the local sediment transport rate and the local mean velocity.



EXPLANATION

Fr = Froude number

λ = wavelength of bedform

$j = \delta/y_0$

y_0 = flow depth

δ = lag distance of the local sediment transport rate and the local velocity

Figure 2.6.—Bedform predictor developed by Kennedy (1969) based on potential flow model

Znameskaya (1969) proposed a plot of Froude number versus dimensionless mean velocity (figure 2.7). Hill and others (1967) plot the shear velocity Reynolds number with a dimensionless grain size (figure 2.8). Vanoni (1974) has a set of graphs (subset shown in figure 2.9) that he used to discriminate among bedforms, with each graph using the Froude number and a dimensionless grain size as the parameters, and the selection of the graph to use being dependent on the grain size median diameter and a dimensionless parameter defined as

$$R_g = \frac{\sqrt{gDD}}{\nu} \quad , \quad [2.1]$$

where g is the acceleration of gravity, D is the grain size, and ν is the kinematic viscosity.

van Rijn (1984C) used a dimensionless grain size ($D_* = R_{ep}^{2/3}$) and plotted it against a transport stage parameter, T (figure 2.10), as

$$T = \frac{u'^2 - u_{*cr}^2}{u_{*cr}^2}, \quad [2.2]$$

where u'_* is the grain shear velocity and u_{*cr} is the critical shear velocity as determined from Shields diagram (van Rijn, 1984A).

Karim (1995) developed bedform regime predictors in the form of limiting Froude numbers, defined as

$$F_t = 2.716 \left(\frac{H}{D_{50}} \right)^{-0.25}, \quad F_u = 4.785 \left(\frac{H}{D_{50}} \right)^{-0.27}, \quad [2.3]$$

where F_t is the beginning of the transition regime (from the lower-flow regime), and F_u is the beginning of the upper regime. Based on these definitions for limiting Froude numbers, the bedform geometry type can be determined as the following.

Lower regime (ripples, dunes)

$$Fr \leq F_t$$

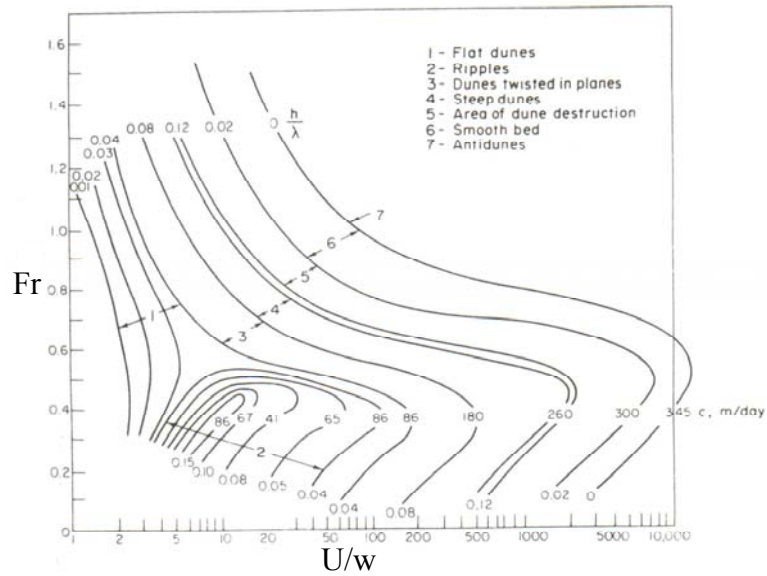
Transition regime (washed out dunes)

$$F_t \leq Fr \leq F_u$$

Upper regime (plane bed, antidunes)

$$Fr \geq F_u$$

Karim (1995) also used $Fr \geq 0.8$ as a predictor for antidunes.



EXPLANATION

- Fr=Froude Number
- U=mean velocity
- w=fall velocity of sediment
- h = dune height
- λ =dune wavelength
- c=dune translation velocity

Figure 2.7.—Bedform predictor proposed by Znamenskaya (1969) (from Raudkivi, 1990)

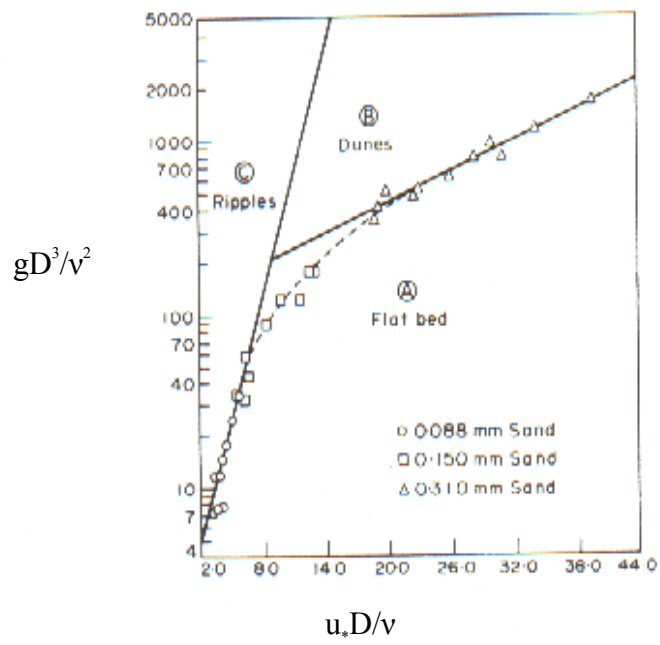
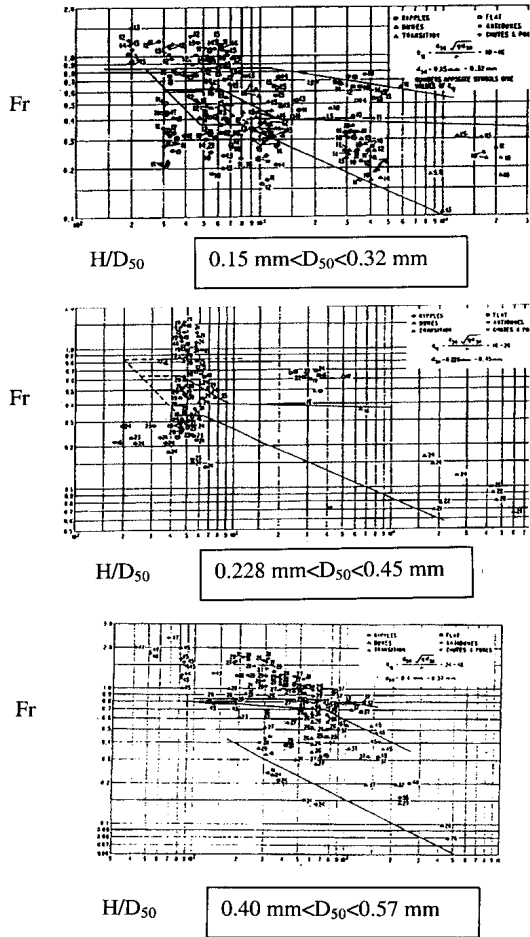


Figure 2.8.--- Bedform predictor proposed by Hill and others (1967) (from Raudkivi, 1990)



EXPLANATION

H = flow depth

D₅₀ = median grain size

Fr = Froude number

Figure 2.9.—Froude number versus H/D₅₀ with indications of the type of bedform present for sands (from Vanoni, 1974)

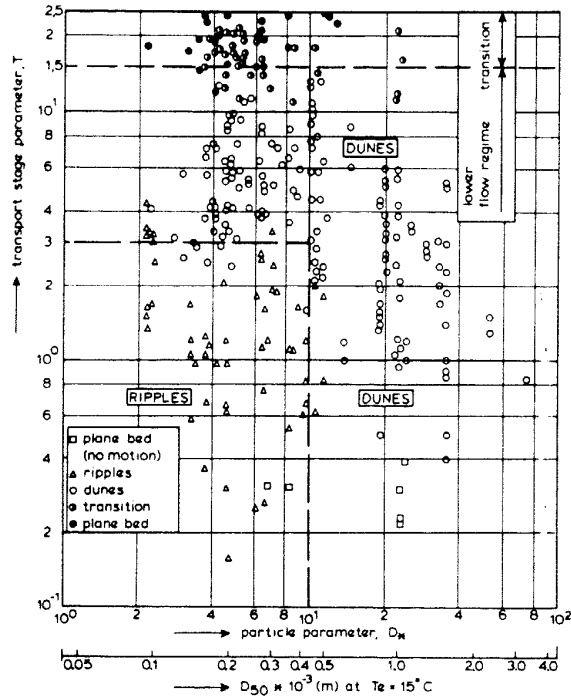


Figure 2.10.—Bedform classification proposed by van Rijn (1984C)

Ripples are reported to occur for hydraulically smooth conditions (Yalin and da Silva, 2001) which requires a viscous (or laminar) sublayer. Rouse (1957) defines the height of the viscous sublayer, δ_v , as

$$\delta_v = 11.6 \frac{\nu}{u_*} \quad . \quad [2.4]$$

From this definition of viscous sublayer, Garcia (1999) reports the criteria for the presence of ripples as

$$\frac{u_* D}{\nu} \leq 11.6 \quad , \quad [2.5]$$

where D is the diameter of the grains. Raudkivi (1990) reports that ripples only develop in fine grained sediments ($D < 0.7$ to 0.9 mm) and at shear velocity Reynold's numbers ($Re_* = \frac{u_* D}{\nu}$) less than 22 to 27, whereas Richards (1980) gave the following criteria for ripple formation

$$0.0007 < kz_0 < 0.16 \quad ,$$

where k is the wave number ($2\pi/\lambda$) and z_0 is the roughness length parameter defined as

$$z_0 = 26.3 \frac{\tau_0 - \tau_c}{(\rho_s - \rho)g} - k_n \quad , \quad [2.6]$$

with k_n the Nikuradse roughness height. Karim (1999) developed a relation for predicting ripples from laboratory data reported by Guy and others (1966). He found that ripples would only occur if

$$N_* < 80 \quad , \quad [2.7]$$

where $N_* = \frac{u_* D_{50}}{\nu} \frac{U}{\sqrt{gRD_{50}}}$, where D_{50} is the median grain size . Finally, Raudkivi

(1997) provides a relation for the occurrence of ripples based on the shear Reynolds number, Re_* (referred to as the boundary Reynolds number by Karim, 1999), where in order for ripples to occur, $Re_* = 10$ to 20 , where

$$Re_* = \frac{u_* D_{50}}{\nu} \quad . \quad [2.8]$$

In much of this discussion so far, little attention has been paid to the effect of water temperature on the type of bedform, although in some cases, this effect is accounted for in the kinematic viscosity in the Reynolds number. Many investigators have noted the effect of water temperature on the alluvial bed resistance, which has been used as an indicator of the type of bedform present (Colby and Scott, 1965, p 12), and sediment transport rate (Straub and others, 1958; Colby, 1964; Burke, 1966; Toffaleti, 1968; and Shen and others, 1978). A few degrees change in temperature can cause the bed configuration to change between flat bed and dune-ripples regime (Vanoni, 1974). Water temperature affects the fluid viscosity, which, in turn, affects the fall velocities of the sediment particles. This affects the mobility of the sediment particles that control the bedform features (Vanoni, 1974). Investigation into the precise effect of water temperature on sediment transport has conflicting conclusions, with Hubbell and Al-Shaikh Ali (1961) concluding that increasing water temperatures either could increase or decrease sediment transport rate. The U.S. Army Corps of Engineers noted a change of bedform with temperature at constant discharges on the Missouri River (U.S. Army Corps of Engineers 1967, 1968, and 1969). In a follow-up study, Shen and others (1978) demonstrated that the curves of Vanoni (1974) are reasonable at picking up this temperature effect for data from the Missouri River.

2.1.2.2 Empirical Predictors of Bedform Geometry

Empirical investigations nearly always start from dimensional analysis to determine the important dimensionless parameters affecting bedform geometry, and proceed to using graphical and multiple regression techniques to determine relations between the bedform geometry and the dimensionless variables. Among the independent parameters, which are made non-dimensional in the analysis, are flow depth (H), Shields stress (or non-dimensional bed shear stress, $\tau_* = \frac{\tau}{\rho R g D}$), grain size (D), water viscosity (ν),

submerged specific gravity ($R = \frac{\rho_s - \rho}{\rho}$), and bed porosity (p).

Yalin (1977A), in an empirical investigation, presents the following expressions that characterize the dimensional analysis of the bedform geometry problem

$$\frac{\lambda}{D} = f\left[\frac{u_* D}{\nu}\right], \text{ for ripples,} \quad [2.9]$$

$$\frac{\lambda}{H} = f\left[\frac{u_* D}{\nu}, \frac{H}{D}\right], \text{ for dunes,} \quad [2.10]$$

$$\frac{H_d}{\lambda} = f\left[\frac{\tau_*}{\tau_{cr}}\right], \text{ for ripples, and} \quad [2.11]$$

$$\frac{H_d}{\lambda} = f \left[\frac{\tau_*}{\tau_{cr}}, \frac{u_* D}{\nu}, \frac{H}{D} \right], \text{ for dunes,} \quad [2.12]$$

where $\frac{u_* D}{\nu}$ is the boundary Reynolds number (Re_*) (also sometimes referred to as the particle Reynolds number). Graf (1971, p. 283) contends that Yalin presented these in his original 1964 work by “making some experimentally unsupported assumption, (from which) dimensionless variables for height (H_d) and length (λ) of bedforms were derived, and the functional relations were obtained from experimental data.” After many experiments, Yalin (1964) established that

$$\frac{H_d}{H} = \frac{1}{6} \left(1 - \frac{H_{cr}}{H} \right), \quad [2.13]$$

and because H_{cr} (depth at which incipient motion takes place) cannot exceed H , it is obvious that H_d/H cannot exceed $1/6$. Garcia (1999) states this as

$$\frac{H_d}{H} < \frac{1}{6} \quad . \quad [2.14]$$

Nordin and Algert (1965) suggests that $1/3$ should be used instead of $1/6$, as the Rio Grande dune heights are closer to one-third the depth.

For ripples, Yalin (1964) determined from extensive laboratory data that for ripples,

$$\lambda=1000D \quad . \quad [2.15]$$

Richards (1980) also indicated an independence of the ripple length from flow properties and surmised the following for ripple length

$$203D < \lambda < 4050D \quad .$$

For wavelets (the precursors of ripples and dunes), Coleman and Eling (2000) give the following relation for their length in both laminar and turbulent flows (correcting the earlier formula of Coleman and Melville (1996) that was only valid for turbulent flow) as

$$\lambda=175D^{0.75} \quad . \quad [2.16]$$

For dunes, Yalin (1964) showed that as Re^* increases, the following applies,

$$\lambda=2\pi H \quad . \quad [2.17]$$

This relation is similar to Hino (1968) who estimated the “prevailing dune length” as

$$\lambda \approx 7H \quad .$$

Allen (1970) suggested that for deep flows ($H > 10m$)

$$\lambda = 1.16H^{1.55} \quad [2.18]$$

For the steepness of dunes and ripples, Yalin (1977A) presents two graphs that plot H_d/λ versus ratio of the Shields stress and the critical Shields stress. Dunes where $Re^* > 31.62$ and $H/D > 100$ are illustrated in figure 2.11, whereas for ripples with $Re^* < 10$ and $H/D > 400$ are illustrated in figure 2.12.

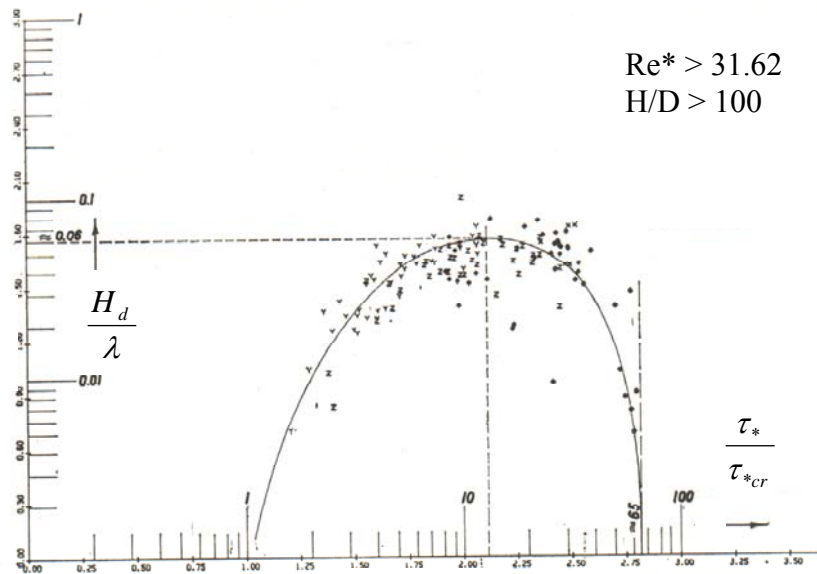


Figure 2.11—Prediction of dune steepness proposed by Yalin (1977A)

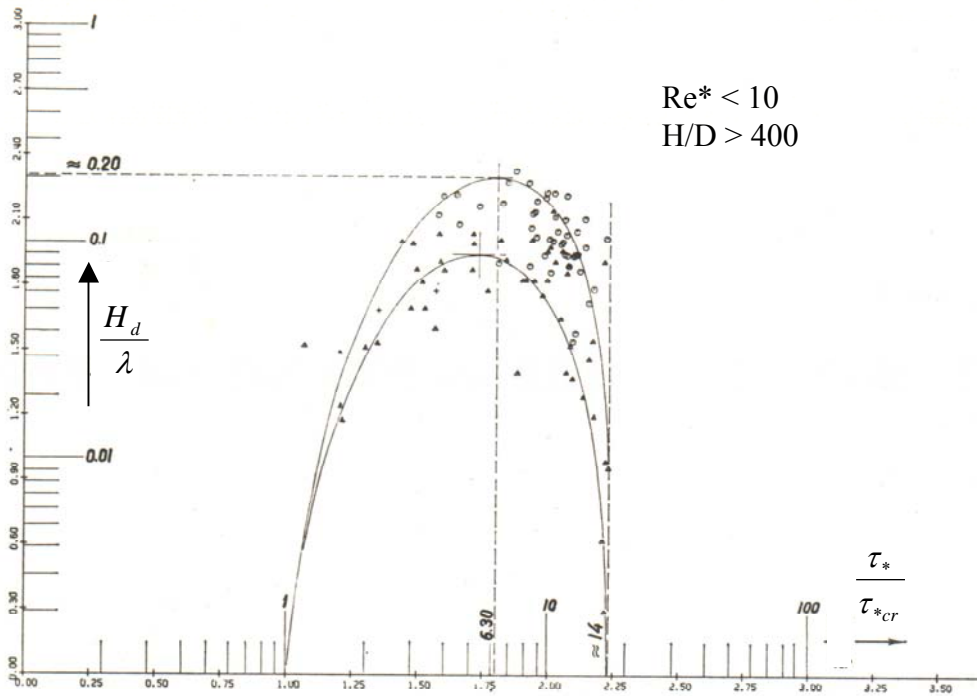


Figure 2.12---Prediction of ripple steepness proposed by Yalin (1977A)

Fredsoe (1975) related dune steepness to shear stresses by suggesting the following equation

$$\frac{H_d}{\lambda} = \frac{1}{8.4} \left[1 - \frac{0.06}{\tau_*} - 0.4\tau_* \right]^2 \quad [2.19]$$

Van Rijn (1984C) gives relations for dune geometry that are some of the most widely used and quoted in the literature. Using 84 sets of data from flume experiments (size ranges from 0.19 to 2.3 mm) and 22 sets of river data (ranging in size from 0.49 to 3.6 mm), van Rijn produced the following empirical equations

$$\frac{H_d}{H} = 0.11 \left(\frac{D_{50}}{H} \right)^{0.3} (1 - e^{-0.5T})(25 - T) \quad , \quad [2.20]$$

$$\frac{H_d}{\lambda} = 0.015 \left(\frac{D_{50}}{H} \right)^{0.3} (1 - e^{-0.5T})(25 - T) \quad , \quad [2.21]$$

where T is the transport stage parameter given above. Van Rijn makes the assumption that for $T < 0$ and $T > 25$, the bed surface almost is flat (he does not consider antidunes). The above relations with the data used to evaluate them are plotted in figures 2.13 and 2.14. From these equations, an expression for the bedform length can be derived as

$$\lambda = 7.3H \quad . \quad [2.22]$$

This equation is similar to Yalin's (1964) expression of $\lambda = 2\pi H$ (equation 2.17).

| | source | flow velocity \bar{u} (m/s) | flow depth d (m) | particle size D_{50} (μm) | temperature T_e ($^{\circ}\text{C}$) |
|------------|---------------------|-------------------------------|------------------|--|--|
| flume data | o Guy et al | 0.34 - 1.17 | 0.16 - 0.32 | 190 | 8 - 34 |
| | x Guy et al | 0.41 - 0.65 | 0.14 - 0.34 | 270 | 8 - 34 |
| | A Guy et al | 0.47 - 1.15 | 0.16 - 0.32 | 280 | 8 - 34 |
| | b Guy et al | 0.77 - 0.98 | 0.16 | 330 | 8 - 34 |
| | □ Guy et al | 0.48 - 1.00 | 0.10 - 0.25 | 450 | 8 - 34 |
| | φ Guy et al | 0.53 - 1.15 | 0.12 - 0.34 | 930 | 8 - 34 |
| | ● Williams | 0.54 - 1.06 | 0.15 - 0.22 | 1350 | 25 - 28 |
| | ▧ Delft Hydr. Lab. | 0.45 - 0.87 | 0.26 - 0.49 | 790 | 12 - 18 |
| | ◊ Stein | 0.52 - 0.95 | 0.24 - 0.31 | 400 | 20 - 26 |
| | ◊ Znamenskaya | 0.53 - 0.80 | 0.11 - 0.21 | 800 | - |
| field data | ● Dutch Rivers | 0.85 - 1.55 | 4.4 - 9.5 | 490 - 3600 | 15 - 20 |
| | ▧ Rio Parana | 1.0 | 12.7 | 400 | - |
| | ◆ Japanese Channels | 0.53 - 0.89 | 0.25 - 0.88 | 1100 - 2300 | - |
| | ■ Mississippi River | 1.35 - 1.45 | 6 - 16 | 350 - 550 | - |

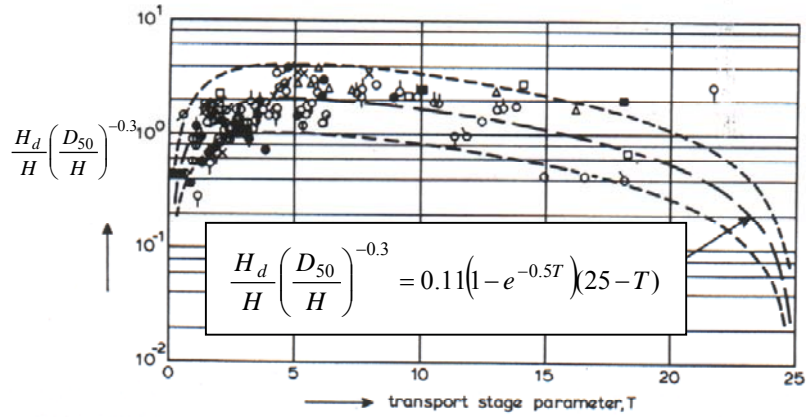


Figure 2.13.—Bedform height predictor proposed by van Rijn (1984C)

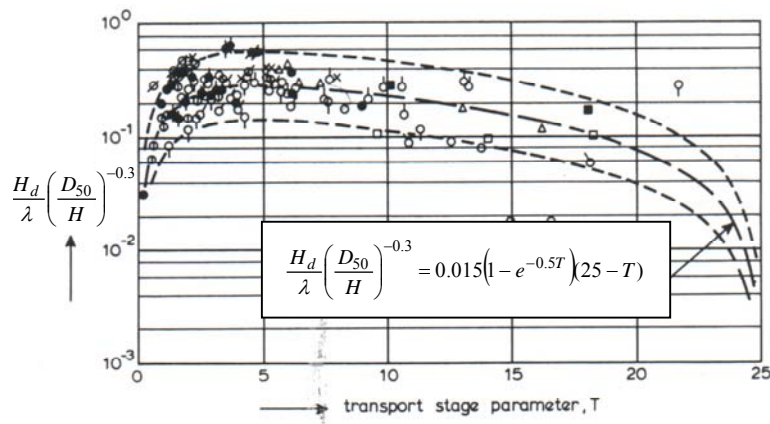


Figure 2.14.---Bedform steepness predictor proposed by van Rijn (1984C)

Julien and Klaassen (1995) analyzed a large amount of field and laboratory data and proposed the following relation

$$H_d = \xi H \left(\frac{D_{50}}{H} \right)^{0.3}, \quad [2.23]$$

where ξ is the dune-height coefficient. Julien and Klaasen report that the average value of ξ is approximately 2.5 and that 95% of their data are reported to be within $0.8 < \xi < 8$.

The dune length is described by

$$\lambda = \eta H_d \left(\frac{H}{D_{50}} \right)^{0.3}, \quad [2.24]$$

where η is a dune-length coefficient with a reported average value of approximately 2.5. Julien and Klaasen indicate that 95% of the data points are within $0.5 < \eta < 8$. When the above two equations are combined and average values for η and ξ are used, Julien and Klaassen give a reasonable first approximation for dune wavelength as

$$\lambda \approx 6.25H. \quad [2.25]$$

Amsler and Garcia (1997) in a discussion of the work of Julien and Klaasen (1995) noted that Julien and Klaasen's data indicated that the large dune heights increased with increasing discharge (shear stress), which was counter to what had been observed on the Parana River in Argentina. Amsler and Garcia (1997) speculated that Julien and Klaasen mistakenly had lumped the small-superimposed dunes (Julien and Klaasen termed these

megaripples) onto the large dunes and, in reality, the large dunes actually decrease. They further state that the predictors of large dunes cannot predict the characteristics of the small dunes (megaripples).

2.1.2.3 Analytic Predictors of Bedform Geometry

Another class of bedform investigation is that of analytical or theoretical models. Most of these models have used linear-stability analysis to determine the stability of small-amplitude sinusoidal bed features. Among the first investigations of this type and best known is that of Kennedy (1963, 1969) who developed an analytical model of potential flow over a wavy bed surface.

Kennedy (1963), using a potential flow formulation of free-surface flow over a sinusoidal bed, derived the following equation to determine the wavelength of the dune

$$Fr^2 = \frac{U^2}{gH} = \frac{1 + kH \tanh(kH) + k\delta \cot(k\delta)}{(kH)^2 + (2 + k\delta \cot(k\delta))kH \tanh(kH)} \quad , \quad [2.26]$$

where Fr is the Froude number, k is the wave number ($2\pi/\lambda$), λ is the wavelength, and δ is the phase shift between the local sediment discharge and local near-bed velocity. The phase shift is the most important concept of Kennedy's analysis and he emphasizes it as a

physical reality and not just an “artifice introduced to achieve the desired prediction” (Kennedy, 1969). However, Raudkivi (1990, p 98) states that evidence for this result is lacking. Fredsoe (1982) gives the following relation for the phase shift

$$\delta = \frac{\varepsilon U_b}{v_s^2} \quad , \quad [2.27]$$

where U_b is the “slip velocity” at the bed, which is given as $U_b \approx u_*$, ε is the eddy viscosity taken as constant over the depth and given by the following $\varepsilon = 0.077 u_* H$, and v_s is the fall velocity. Kennedy and Odgaard (1991) acknowledge that because the method was developed using linearized (small wave amplitude) theory, Kennedy’s (1963) method is of limited value in analyzing fully developed bedforms.

Coleman and Fenton (1996), without using a phase shift, concluded that equation 1.10, formerly used to delineate between antidunes and dune/ripple bedforms, is valid to use as a predictor of wavelength for flows where $Fr < 0.8$.

Fredsoe (1982) used perturbation methods to arrive at relations for the dune height and wavelength as functions of sediment transport, shear stress, and water depth. In developing the method, a small perturbation was introduced on the dune and conditions were examined under which the dune was stable. The bedform height is given by

$$\frac{H_d/H}{\left(1 - \frac{H_d}{2H}\right)} = \frac{\Phi_b}{2\theta \left(\frac{d\Phi_b}{d\theta} + \frac{d\Phi_s}{d\theta}\right)} \quad , \quad [2.28]$$

where Φ_b is the dimensionless bedload sediment transport, Φ_s is the dimensionless suspended sediment transport, θ is the bed shear stress near the top of the dune (which scales with the dimensionless grain shear stress τ'_*). The equations for these dimensionless quantities are

$$\Phi_b = \frac{q_b}{\sqrt{RgD^3}} \quad , \quad [2.29]$$

$$\Phi_s = \frac{q_s}{\sqrt{RgD^3}} \quad , \quad [2.30]$$

$$\tau'_* = \frac{\tau'_0}{\rho RgD} \quad , \text{ and} \quad [2.31]$$

$$\Phi_b = f(\tau'_*) \quad , \quad [2.32]$$

where q_b is the bed load transport, q_s is the suspended-sediment load, R is the submerged specific gravity, ρ is the water density, and D is the mean grain diameter. The relation between H_d/H and the dimensionless shear stress is shown in figure 2.15. At low dimensionless shear stress, one curve represents all grain sizes. This one curve is indicative that only bedload is transporting sediment. At the higher shear stresses, suspended sediment becomes in the geometry of the bedform.

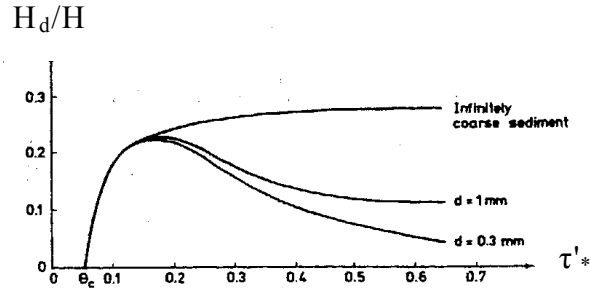


Figure 2.15.—Bed shear stress as a predictor of dune height as proposed by Fredsoe (1982)

Fredsoe (1982) gives the following relation for the dune wavelength

$$\lambda = \frac{[16H_d q_b + (16H_d + \delta)q_s]}{(q_b + q_s)} \quad , \quad [2.33]$$

where δ is the phase shift and is computed as in equation 2.27. Figure 2.16 depicts the variation in H_d/λ with dimensionless shear stress.

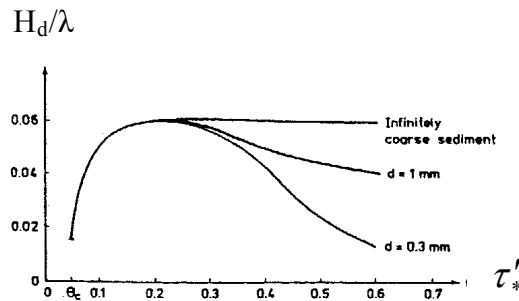


Figure 2.16.--- Bed shear stress as a predictor of dune steepness as proposed by Fredsoe (1982)

Haque and Mahmood (1985) developed a non-dimensional graph of bedform shape from two-dimensional boundary value potential flow analysis. Plots of data collected in canals and rivers in Pakistan are shown in figure 2.17.

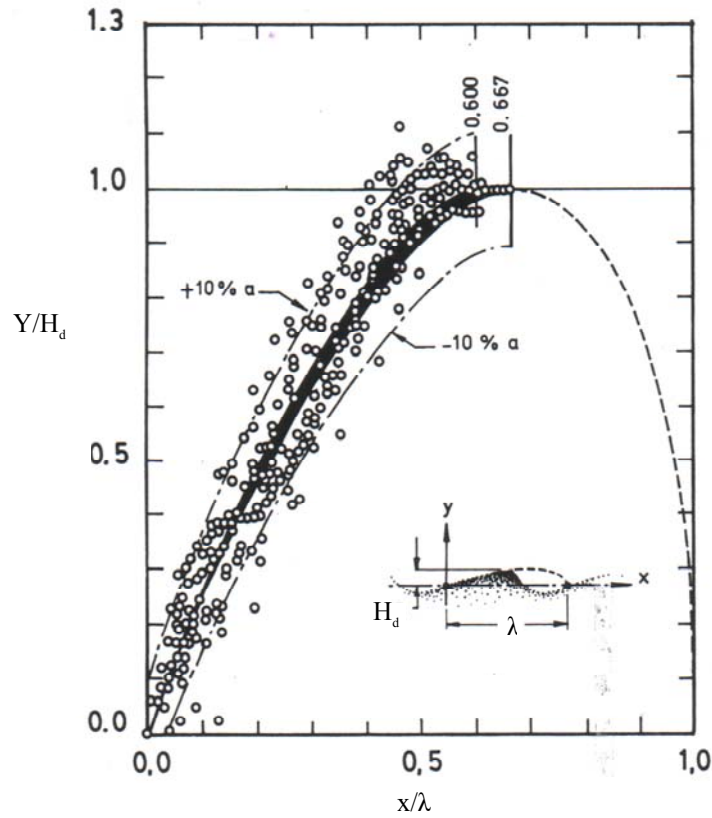


Figure 2.17.---Comparison of theoretical and observed bedform shapes (from Haque and Mahmood, 1985)

Kennedy and Odgaard (1991) proposed the following analytical relation

$$\frac{H_d}{H} = \frac{1}{2} \left\{ \frac{1.2A\alpha f_0}{8C_D} + \left[\left(\frac{1.2A\alpha f_0}{8C_D} \right)^2 + \frac{2\pi Fr^2 f_0}{C_D C_1} \left(\frac{f}{f_0} - \frac{1.2A}{2} \right) \right]^{1/2} \right\}, \quad [2.34a]$$

where f_0 is the rigid-flat-bed Darcy-Weisbach friction factor,

$$f_0 = \frac{8}{\left\{ 6.25 + 2.5 \ln \left(\frac{H}{2.5D_{50}} \right) \right\}^2}, \quad [2.34b]$$

f is the Darcy-Weisbach friction factor; Fr is the Froude number; $A=1.0$; $C_D=1.0$; $\alpha=5$; and $C_1=0.25$. Equation 2.34a was derived by following the concept of relating energy slope (because of form drag) to head loss across an abrupt expansion in a conduit.

Karim (1999), used a similar concept to that of Kennedy and Odgaard (1991), whereby energy loss because of form drag is related to the head loss across a sudden expansion in an open channel. Karim presents the following equation for the geometry of ripples, dunes, and transition bedforms as

$$\frac{H_d}{H} = \left[\frac{\left\{ S_e - 0.0168 \left(\frac{D_{50}}{H} \right)^{0.33} Fr^2 \right\} \left(\frac{\lambda}{H} \right)^{1.20}}{0.47 Fr^2} \right]^{0.73}, \quad [2.35]$$

where S_e is the energy slope. Karim further recommends to solve for λ/H using the equation of Julien and Klaassen (1995) ($\lambda/H=6.25$) for dunes and Yalin's (1964) relation for ripples ($\lambda=1000 D$) (equation 2.15).

2.2. Flow Over Bedforms

The velocity in a shear flow is non-uniform because of the presence of the boundary and the resulting resistance to flow not only along the boundary but between the fluid particles. Although it was realized as early as 4th century B.C. by Aristotle that flow resistance was important to the bulk flow (Rouse and Ince, 1963), it was not until Prandtl (1904) presented his paper on boundary layer theory that fluid mechanics was incorporated into flow-resistance theory and enabled a characterization of the profile of the velocity distribution in the vertical (Yen, 1992). Alluvial channels add a layer of complexity to any investigation into the flow field because of the capacity of the boundary geometry to change with flow condition. In laboratory experimental observations, it has been noted that in flow over a train of bedforms, a definitive momentum defect region is observed (Nelson and others, 1993; Bennett and Best, 1995). The region is associated with flow separation and wake formation downstream of the bedform lee face and as the wake is advected downstream, the effect of the momentum defect is diffused outward, causing the region to grow in depth. A conceptual drawing of the flow character in the presence of bedforms is given in figure 1.1. The flow separates at the crest of the bedform and reattaches at some point downstream on the next bedform. This flow over the bedforms creates an adverse pressure gradient

$$\left(\frac{\partial^2 u}{\partial z^2} \Big|_{z=0} = \frac{1}{\mu} \frac{dp}{dx} > 0 \right)$$

that causes a smaller velocity gradient and, thus, a smaller velocity near the bed. Results from laboratory investigations of Shen and others (1990) that demonstrate this adverse pressure gradient are shown in figure 2.18. The reduction in velocity at the bed in the presence of these adverse pressure gradients is well

demonstrated on the stoss side of the bedform in figure 2.19 reproduced from Nelson and others (1993).

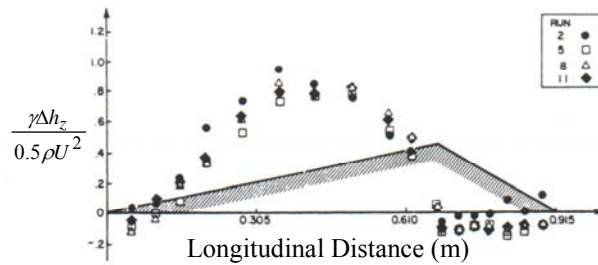


Figure 2.18.—Non-dimensional pressure distribution in flow over a bedform (from Shen and others, 1990)

For alluvial channels with bedforms, the flow resistance often is partitioned into form resistance and grain resistance. This partitioning is important to do when considering sediment transport, as the grain resistance is the only component that affects the motion of the sediment grains (Garcia, 1999, p. 6.47).

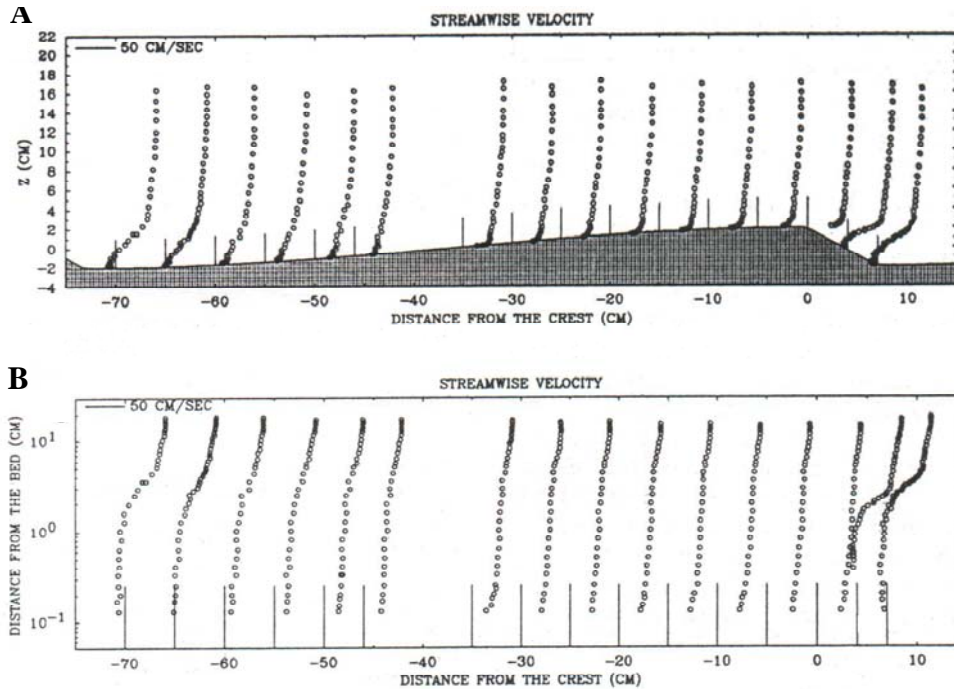
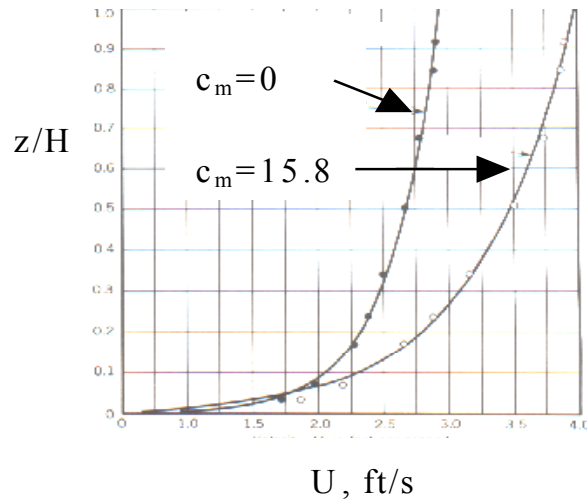


Figure 2.19.—Observations of velocity distribution along a bedform plotted both in A) linear and B) log space by Nelson and others (1993)

For a typical shear flow over a flat-rough bed, the velocity profile (figure 2.20) typically is approximated with one logarithmic equation for the entire depth of the flow (although it is acknowledged that this is in violation of the assumptions inherent in the log law of the wall). The Reynolds stresses typically decrease monotonically away from the boundary, reaching zero near the water surface in equilibrium conditions. With bedforms present, the velocity and Reynolds stress profiles (figures 2.19 and 2.21) have been shown experimentally to be different from those for a plane bed (Bennett and Best, 1995; Nezu and Nakagawa, 1993). The velocity profiles for these experiments were logarithmic in nature; however, the slopes vary in at least two separate distinct layers. The separation point between the layers corresponds to a maximum in the Reynolds stress, where the Reynolds stress increases from the boundary to the location of the

maximum shear stress then decreases toward the water surface. Fedele and Garcia (2001) refer to this as the equilibrium or reference layer (ϵ_e).



c_m = the sediment discharge concentration of the flow, which when multiplied by the flow rate, will give the total concentration of the flow

Figure 2.20.-Velocity profiles in a typical shear flow (Vanoni, 1975)

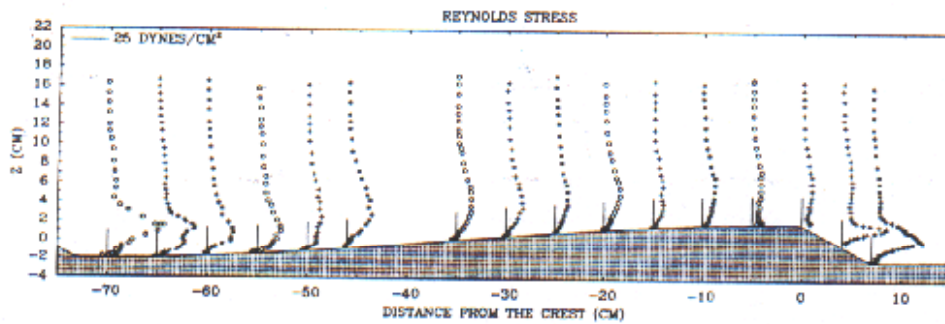


Figure 2.21.--- Observations of Reynold stress distribution along a bedform (Nelson and others, 1993)

2.2.1 Flow Resistance and Shear Partitioning Models

Flow resistance research in rigid conduit flow began in earnest with the work of Bazin (1865) and Darcy (1857), with major contributions by Nikuradse (1933) for pipe flow and Moody (1944). Blasius (1913), a student of Prandtl's, proposed that the resistance coefficient f was related to a quantity that is now known as the Reynold's number, $Re=UR_h/\nu$ (Carter and others, 1963), where for flows of $700 < Re < 30,000$ the friction factor is expressed as:

$$f = \left(\frac{0.224}{(Re)^{0.25}} \right) \quad . \quad [2.36]$$

According to Carter and others (1963), Hopf (1923) and Fromm(1923) published the first papers on the measurement of roughness coefficients that included modern fluid-mechanics concepts. Hopf showed that f was a function of Re , relative roughness, and cross-sectional shape.

The works of Prandtl (1925) and Von Karman (1931) have led to the introduction of an additional formula for f for smooth pipe flow as a function of Re . An excellent discussion of this derivation and its utilization of Boussinesq's (1877) work is found in Tracy and Lester (1961, p. 2-5). The equation, known as the Prandtl-Von Karman resistance formula for smooth flow, presented here is

$$\frac{1}{\sqrt{f}} = 2.03 \log(Re\sqrt{f}) - 1.08 \quad , \quad [2.37]$$

where Re for the half section of an infinitely wide, smooth conduit is $\frac{4R_h U}{\nu}$.

Nikuradse (1933) presented his classical work in which he had meticulously glued sand particles of uniform size to the inside of pipes and determined the f through the partly rough flow region. Since this work, boundary roughness for impervious rigid walls is often expressed as an equivalent sand grain size, k_s . Colebrook and White (1937) investigated the same partly rough flow region with non-uniform roughness elements. Colebrook (1938) introduced the familiar Colebrook-White equation as

$$\frac{1}{\sqrt{f}} = -2 \log \left(\frac{k_s}{14.83 R_h} + \frac{2.52}{Re \sqrt{f}} \right) \quad [2.38]$$

The well known Moody diagram is only for pipe flow. As Yen (1992) points out, no valid Moody type diagram has been developed for open-channel flow. Rouse (1943) presented results that plotted $\frac{1}{\sqrt{f}}$ vs. $\frac{Re}{\sqrt{f}}$. Moody suggested that Rouse use f vs Re as the primary scales (Yen, 1992). When Rouse refused to do this, Moody (1944) presented a plot, known as the Moody diagram, which is used widely today. This diagram is used iteratively by computing the relative roughness (ϵ_s/D), assuming a velocity, calculating the Re from this velocity, and determining the value of f from the diagram. ϵ_s is the equivalent sand diameter (analogous to Nikuradse's k_s) and D is the pipe diameter. The value of the resistance coefficient is plugged into the Darcy-Weisbach equation (equation 1.2) and a velocity is computed. From this velocity, Re is computed and checked against the Re from the assumed velocity. This process is repeated until

successive Re's match. At large Reynolds numbers (1×10^4 to 1×10^7 , depending on relative roughness), the resistance coefficient becomes independent of Re and only a function of the relative roughness. This property of the Moody diagram is consistent with the equations presented earlier (equations 2.36, 2.37, 2.38).

Yen (1992) presents a basic preliminary "Moody-type" diagram for steady-uniform open channel flow. His plot only deals with the areas of the diagram where the flow is either in the laminar region or the fully turbulent high-Reynolds number region. Brownlie (1981) also presents a "Moody-type" graph based on the data of Nikuradse and purports its use for open-channel flows.

In determining the grain-resistance coefficients, many investigators have tried to borrow from Nikuradse's equivalent grain roughness concepts and relate the resistance to some measure of k_s . Rouse (1946) suggested that Manning's n , if it is indeed independent of Re , should be related to some measure of wall roughness as

$$n = C_n k_s^{\frac{1}{6}}, \quad [2.39]$$

where C_n is a constant of proportionality. Various investigators have proposed various relations of bed material size to k_s . Yen (1992) presented a table (table 2.3 below) that summarizes the various equations that investigators have proposed to determine the value of k_s ; these equations being of the form

$$k_s = \alpha_s d_x, \quad [2.40]$$

where α_s is a proportionality constant, and d_x is the reference sediment size.

| Investigator | d_x | α_s |
|--------------------------------|----------|------------|
| Ackers and White (1973) | d_{35} | 1.23 |
| Strickler (1923) | d_{50} | 3.3 |
| Keulegan (1938) | d_{50} | 1 |
| Meyer-Peter and Muller (1948) | d_{50} | 1 |
| Thompson and Campbell (1979) | d_{50} | 2.0 |
| Hammond and others (1984) | d_{50} | 6.6 |
| Einstein and Barbarossa (1952) | d_{65} | 1 |
| Irmay(1949) | d_{65} | 1.5 |
| Engelund and Hansen (1967) | d_{65} | 2.0 |
| Lane and Carlson (1953) | d_{75} | 3.2 |
| Gladki(1979) | d_{80} | 2.5 |
| Leopold and others (1964) | d_{84} | 3.9 |
| Limerinos(1970) | d_{84} | 2.8 |
| Mahmood(1971) | d_{84} | 5.1 |
| Hey(1979), Bray(1979) | d_{84} | 3.5 |
| Ikeda(1983) | d_{84} | 1.5 |
| Colosimo and others (1986) | d_{84} | 3-6 |
| Whiting and Dietrich (1990) | d_{84} | 2.95 |
| Simons and Richardson (1966) | d_{85} | 1 |
| Kamphuis (1974) | d_{90} | 2.0 |
| van Rijn (1982A) | d_{90} | 3.0 |

Table 2.3. Ratio of Nikuradse equivalent grain roughness size and sediment size for open- channel flows (from Yen, 1992, p. 120)

When considering flat beds in channels with sediment along the bottom, it is worth noting that Karim and Kennedy (1990) found that the friction factors of flows over mobile flat beds were about 20 percent higher than those for flows with rigid beds with the same equivalent roughness length. This follows the same reasoning that Smith and McLean (1977) adopted in assuming that the roughness length (k_s) for sediment-transporting channels is higher than for non-sediment transporting channels. They equate

the roughness length to the sum of the Nikuradse k_s plus the height of the saltating bedload layer.

As non-rigid channels, alluvial channels present new challenges when investigating the flow resistance because the flow forms the boundary but then the boundary, in turn, forms the flow. Simons and Richardson (1966) state:

“Resistance to flow in alluvial channels is complicated by the large number of variables. It is further complicated by the interdependency, either real or apparent, of the variables. In fact, some variables may be altered or even determined by the flow, and changes in flow conditions may change the role of a dependent variable into that of an independent one. It is difficult, especially in field studies, to differentiate between independent and dependent variables.”

Gilbert (1914) performed some of the earliest experiments on alluvial channels and found that the resistance coefficient varied with bedforms. The changes in bedform geometry in river systems have been recognized as accounting for much of the variation in friction factors of natural alluvial streams (Julien and Klaassen, 1995). In the presence of bedforms, Einstein (1950) introduced the most predominant approach to determining the separation of the shear stress because of the presence of bedforms (or flow resistance

because $f = \frac{8g}{U^2} R_h S = 8 \frac{\tau_0}{\rho U^2}$.

Einstein assumed that the shear stress could be separated (partitioned) using linear superposition, where the total bed-shear stress is divided into that induced by the grain roughness and that induced by form resistance as

$$\tau_0 = \tau'_0 + \tau''_0 \quad , \quad [2.41]$$

which leads to

$$f = f' + f'' \quad , \quad [2.42]$$

where τ_0 =total bed shear stress, τ'_0 = grain shear component of the total shear stress, τ''_0 =form drag component of the total bed shear stress, f = total Darcy-Weisbach friction factor, f' = grain shear friction factor, and f'' =form-drag friction factor.

The grain shear friction factor is determined in many cases as the plane-bed friction factor, an approach which is influenced by the work of Nikuradse (1933). The form-drag friction factor then could be determined in experiments as the difference between the total measured friction factor and the grain shear friction factor, although some investigators measured both components separately (Shen and others, 1990; Nelson and others, 1993)

Many investigators have used this linear-superposition treatment to separate or partition the shear stress (or resistance coefficient) (e.g., Einstein and Barbarossa, 1952; Vanoni

and Brooks, 1957; Shen, 1962; Yalin, 1964; Alam and others, 1966; Engelund, 1967; Engelund and Hansen, 1967; Simons and Richardson, 1966; Vanoni and Hwang, 1967; Lovera and Kennedy, 1969; Alam and Kennedy, 1969; Engelund and Fredsoe, 1982; van Rijn, 1982; Nelson and Smith, 1989B; Fedele, 1998; and Fedele and Garcia (2001)). Several investigations have provided further equations to compute one or both sides of equation 2.42. An example of this is the work of Vittal and others (1977). In a laboratory investigation on fixed bedforms, they presented the following equations for the friction factors as

$$f' = \frac{0.0224}{\frac{H_d}{\lambda} \left[\frac{H}{k_s} \text{Re} \right]^{1/6}} \quad \text{for } 0.007 < f' < 0.025 \quad , \quad [2.43]$$

$$f'' = 4C_d \frac{H_d}{\lambda} \quad \text{for } 0.11 \leq H_d/H \leq 0.3; \text{ and } 0.05 \leq H_d/\lambda \leq 0.2 \quad , \quad [2.44]$$

where

H_d is the height of the bedform, H is the average depth, λ is the bedform wavelength, k_s is the grain roughness length (set equal to the D_{65} of the bed material), Re is the Reynolds number of the flow (UH/ν), U is the mean velocity of the flow, ν is the kinematic viscosity of the fluid, and C_d is the drag coefficient.

The shear-partitioning method of Einstein (1950) requires knowledge of the total boundary shear stress to carry out the computations necessary for computation of the

component stresses. Einstein and Barbarossa (1952) developed a method using empirical data that allowed one to partition the shear stresses and, thus, resistance coefficients, without the knowledge of the total shear stress. Starting with the assumption given in equation 2.41 and further assuming that the hydraulic radius and the area of the flow could be divided similarly by

$$R_h = R'_h + R''_h \quad , \quad [2.45]$$

$$A = A' + A'' \quad , \quad [2.46]$$

then by use of Manning's equation (equation 1.1) and Strickler's empirical resistance coefficient equation gives

$$n = \frac{\sqrt[6]{k_s}}{29.3} \quad . \quad [2.47]$$

Einstein and Barbarossa (1952) determined that the ratio of the mean velocity and grain roughness shear velocity is

$$\frac{U}{u'_*} = 7.66 \left(\frac{R'_h}{k_s} \right)^{1/6} \quad , \quad [2.48]$$

where $u'_* = \sqrt{gR'S}$ and $k_s = D_{65}$.

In cases where the grain roughness does not produce a hydraulically rough surface (ratio of roughness diameter to theoretical thickness of the viscous sublayer $(\frac{k_s u'_*}{11.6\nu})$ is less

than 5, a logarithmic formula was recommended with a correction factor taken from figure 2 in the Einstein and Barbarossa (1952) paper. Einstein and Barbarossa (1952) also provide a graph (figure 3 in the their paper), derived from field data on the Missouri River Basin and California streams, that relates u_*'' to ψ' (Einstein, 1942), where

$$\psi' = \frac{\rho_s - \rho}{\rho} \frac{D}{R_h' S} \quad . \quad [2.49]$$

This graphical relation has come to be known as the bar-resistance graph in the literature. From these relations, the total resistance coefficient can be obtained by following the steps below.

1. Knowing the cross section properties, slope of channel, and bed sediment size, determine a value of R_h' (use H' for wide channels).
2. Calculate u_*' and ψ' from $u_*' = \sqrt{gR'S}$ and equation 2.49.
3. Determine U from equation 2.48 .
4. Obtain U/u_*'' from the figure in Einstein and Barbarossa (1952) (which depends on ψ') and calculate H'' (or R_h'') from u_*'' .
5. Calculate the value of $H=H'+H''$ (or $R_h=R_h'+R_h''$) .
6. For this value of H (or R_h), the total shear velocity u_*^2 is equal to

$$u_*'^2 + u_*''^2 \text{ . Thus, the resistance coefficient is } \sqrt{\frac{f}{8}} = \frac{u_*}{U} \text{ .}$$

The partition method of Engelund and Hansen (1967) is similar to that of Einstein and Barbarossa (1952) with the exception that they directly relate the dimensionless total shear stress, τ_* , to the dimensionless grain shear stress, τ'_* , where

$$\tau_* = \frac{\tau_0}{\rho R g D}, \quad \tau'_* = \frac{\tau'_0}{\rho R g D}, \quad [2.50]$$

ρ is the fluid density, R is the submerged specific gravity ($\frac{\rho_s - \rho}{\rho} \cong 1.65$), g is the acceleration of gravity, and D is the grain size.

The Nelson-Smith partition (Smith and McLean, 1977; Wiberg and Nelson, 1992; Nelson and others, 1993) of the shear stress also use the linear superposition idea introduced by Einstein; however, they approach the problem from a fluid dynamics analysis of the drag introduced by the bedform. Based on various experiments, the Nelson-Smith partition method introduces the form drag as

$$D_f = B \frac{1}{2} \rho C_d H_d U_r^2, \quad [2.51]$$

where B = channel width, C_d = drag coefficient, ranging from 0.21 (Smith and McLean, 1977) to 0.23 (Wiberg and Nelson, 1992) to 0.25 (Nelson and others, 1993), H_d is the bedform height, and U_r denotes the reference velocity that corresponds to the mean velocity between $z=k_s$ and $z=H_d$ if the bedforms were not present. The form shear stress

can be computed from the form drag divided by the area of the bed over which the force is applied as

$$\tau_0'' = \frac{1}{2} \rho C_d \frac{H_d}{\lambda} U_r^2, \quad [2.52]$$

where λ is the bedform wavelength. From an integration of the logarithmic velocity profile from $z = k_s$ to $z = H_d$, U_r is given by the following equation as

$$\frac{U_r}{u_*'} = \frac{1}{\kappa} \left[\ln \left(30 \frac{H_d}{k_s} - 1 \right) \right]. \quad [2.53]$$

Combining these two equations and assuming partitioning of the shear stress according to that of Einstein (1950) yields

$$\tau_0'' = \tau_0 - \tau_0' = \frac{1}{2} C_d \frac{H_d}{\lambda \kappa^2} \left[\ln \left(30 \frac{H_d}{k_s} - 1 \right) \right]^2 \tau_0' \quad [2.54]$$

Assuming that the total shear stress can be computed from the force balance concepts for equilibrium flow as

$$\tau_0 = \rho g H S. \quad [2.55]$$

Then, with knowledge of the geometry of the bedforms (H_d and λ), the drag coefficient, the grain roughness length, k_s , and the grain shear stress, τ'_0 , can be computed. In turn, the form shear stress can then be computed. The major drawback to using the Smith-Nelson shear partitioning method is the requirement to know the geometry of the bedforms, prior to applying the method.

Nelson and others (1993, p. 3,944) suggest that the interaction of spatial acceleration of the flow over bedforms with the turbulence field is important in altering the form drag of bedforms. This alteration will cause problems with their estimate of the resistance coefficient (C_d) at approximately 0.25; however, they contend that as long as the bedforms are two dimensional with heights of approximately 20% of the flow depth, C_d essentially will be constant. When ripples are present, the drag coefficient will not be constant at around 0.25 (the bedform heights are less than 20% of the flow depth).

2.2.2 Velocity Profile Characterization

In understanding the velocity profile characterization, it is necessary to express the velocity profile relations, discuss the assumptions behind their derivations, and delineate in what parts of the flow are they applicable. According to Yen (1992, p. 15), boundary layer theory provides for the velocity distribution in the vertical direction to be adequately described by two laws or regions of the flow field:

- A) Law of the wall (also termed inner law and applies to the inner-flow region)
- B) Velocity defect law (also termed outer law and applies to the outer-flow region)

For each region, multiple equations potentially satisfy the inner and outer-laws. Whereas each of these laws applies to a region in the flow, it is acknowledged that these regions overlap, also providing for overlap in the application of the pertinent laws.

2.2.2.1 Regions of Flow

In Yen's (1992) classification of the regions of flow, there is an inner region and an outer region. Near the bed, the Reynolds stresses are negligible with the viscous stresses dominating and the local shear stress assumed to be constant and equal to the shear stress at the bed. This thin region near the bed is often termed the laminar (or viscous) sublayer. The viscous sublayer has a linear relation between the velocity and the distance from the bed for the velocity profile. The depth of the viscous sublayer is defined as

$$\delta_v = X \frac{\nu}{u_*}, \quad [2.56]$$

where X has been estimated by various investigators and ranges from 5 to 12.6 (Schlichting (1979, p. 604); Sabersky and others (1989, p. 257); Rouse (1959); Clauser (1956); Julien (1995)). The viscous sublayer only is present in flows that are termed hydraulically smooth or transitionally hydraulically smooth. The idea of a smooth or rough flow regime will be discussed in the next section.

Outside of the viscous sublayer, the inner law layer extends upward and overlaps with the outer layer. As Yen (1992) has defined, the inner region is where “*viscous effects dominate*” and is not deep. In this region, the velocity profile is logarithmic. In many cases, the logarithmic velocity profile is assumed to extend well beyond the top of the inner region (many assume it extends to

the water surface), which is a direct violation of the assumptions made for its derivation (the derivation will be given in the next section).

Yen (1992, p. 18) implies that the outer region extends down to a point near the boundary where

$$z = \frac{30\nu}{u_*} \quad . \quad [2.57]$$

In this outer region, the velocity profile can be shown to be logarithmic, although it has a different form with different scaling.

A classification of the various regions of flow field, based on turbulent structure of the flow, is reported by Nezu and Nakagawa (1993, p. 19). They divide the turbulent structure of the flow into three regions: 1) wall region, 2) intermediate region, and 3) free-surface region. The wall region applies to the part of the flow where $0 \leq z/H < 0.15$ to 0.20 , with velocities and lengths scaled in this region with u_* and ν/u_* , respectively. The free-surface region lies in the range $0.6 \leq z/H \leq 1.0$, where the velocity scales with the maximum velocity, U_m , and the length scales with the flow depth. An intermediate region lies between the wall region and the free-surface region that is not strongly affected by either the wall or the free surface. The velocity and length scales assigned to this region are $\sqrt{\tau/\rho} = u_*$ and H , respectively.

2.2.2.2 Derivations of Turbulent Velocity Relations from Boundary Layer Theory

Boussinesq (1877), Prandtl (1925), and Von Karman (1931) did pioneering work in turbulent boundary layers to provide the framework for much of our theory today on the velocity distributions in a flow field. Boussinesq was the first to advance the hypothesis that a coefficient

analogous to the viscosity in Stokes law for laminar flow was present to describe the stress induced by turbulence (Reynolds Stresses) and that the total shear stress could be written as

$$\tau = \tau_v + \tau_t = \mu \frac{du}{dz} + \mu_t \frac{du}{dz} , \text{ where} \quad [2.58]$$

$$\tau_t = -\overline{\rho u'w'} = \mu_t \frac{du}{dz} = \rho \nu_t \frac{du}{dz} , \quad [2.59]$$

τ_v is the viscous shear stress because of the molecular properties of the fluid, τ_t is the shear stress from turbulence, μ is the dynamic viscosity, μ_t is the dynamic eddy viscosity, ρ is the density, ν_t is the kinematic eddy viscosity, and u' and w' are streamwise and vertical velocity fluctuations, respectively. However, this alone does not help us solve for anything of substance. Prandtl (1925) introduced his mixing length theory that postulated that layers of fluid maintain a constant momentum in the streamwise direction. A lump of fluid is moved to an adjacent layer, by a distance l , and maintains its momentum, despite moving into a new layer. Through derivation and assumptions (detailed in Schlichting, 1979, p 580), it is postulated that

$$\left| \overline{u'} \right| \sim \left| \overline{v'} \right| \sim l \left| \frac{du}{dz} \right| . \quad [2.60]$$

From equations 2.60 and 2.58, yields the following:

$$\tau = \tau_v + \tau_t = \mu \frac{du}{dz} + \rho l^2 \left| \frac{du}{dz} \right| \frac{du}{dz} . \quad [2.61]$$

Separating the du/dz terms (as opposed to just lumping them as a square term) allows for the sign of the turbulent shear stress to change with that of du/dz . This formulation by Prandtl is equivalent to computing the eddy viscosity in Bousinesq's relation as

$$\mu_t = \rho l^2 \left| \frac{du}{dz} \right| . \quad [2.62]$$

Acknowledging that in turbulent flow away from the immediate vicinity of the boundary, the viscous stresses are negligible when compared to the turbulent stresses, the following derivation, attributable to Prandtl, results in:

$$\tau = \tau_t = \rho l^2 \left| \frac{du}{dz} \right| \frac{du}{dz} . \quad [2.63]$$

However, the value for the mixing length remains undetermined. Prandtl assumed that the mixing length scales with the wall distance (Schlichting, 1979, p 587) as

$$l = \kappa z . \quad [2.64]$$

Utilizing equation 2.64 and the assumption that the shear stress near the bed is equal to that at the bed (τ_0) and remains constant (i.e. constant shear stress layer), equation 2.63 becomes

$$\tau_0 = \rho u_*^2 = \rho \kappa^2 z^2 \left| \frac{du}{dz} \right| \frac{du}{dz} \quad . \quad [2.65]$$

Taking the square root of both sides and integrating results in

$$u = \frac{u_*}{\kappa} \ln z + C \quad . \quad [2.66]$$

Equation 2.66 can be recognized as the universal velocity distribution equation (equation 1.5) discussed in section 1.1. When the constant C is evaluated for $u=0$ at $z=z_0$, then

$$C = -\frac{u_*}{\kappa} \ln z_0 \quad . \quad [2.67]$$

Equation 2.66 now can be expressed as

$$u = \frac{u_*}{\kappa} (\ln z - \ln z_0) = \frac{u_*}{\kappa} \ln \left(\frac{z}{z_0} \right) \quad . \quad [2.68]$$

From the assumptions inherent in the development, equation 2.68, in the strictest sense, only is applicable near the boundary. However, equation 2.68 has been applied to flow away from the boundary with fairly good results.

From dimensional analysis arguments, z_0 is proportional to the ratio v/u_* , which can be expressed as

$$z_0 = \beta \frac{\nu}{u_*} \quad . \quad [2.69]$$

Combining 2.68 and 2.69 allows the following equation that Schlichting (1979, p. 589) terms the dimensionless, logarithmic, universal velocity-distribution law as

$$\frac{u}{u_*} = \frac{1}{\kappa} \left(\ln \frac{zu_*}{\nu} - \ln \beta \right) = \frac{1}{\kappa} \ln \frac{zu_*}{\beta \nu} \quad . \quad [2.70]$$

Von Karman's constant, κ , is a universal constant of turbulent flow and equal to about 0.4. Some investigators (Vanoni, 1946; Einstein and Chien, 1955) have reported that κ varied with sediment concentration, however, this variation has been shown (Coleman, 1981; Gelfenbaum and Smith, 1986) to be an artifact of these investigators misapplying the log-law far away from the boundary, which violates the assumptions of the original derivation. The other constant, β , is dependent on the nature of the wall surface.

Two types of boundary conditions (or flow regimes), with a transition zone between them, are known to exist in turbulent shear flows: hydraulically smooth flow and hydraulically rough flow. These flow regimes are characterized by the size of the grain roughness and the depth, δ_v , of the potential viscous (or laminar) sublayer (Julien, 1995, p. 94). The boundary is said to be hydraulically smooth if the grain roughness size (k_s) is less than the viscous sublayer height (δ_v), and hydraulically rough if k_s is larger than δ_v .

For hydraulically smooth fully turbulent flow, experimentally it has been found that

$$-\frac{1}{\kappa} \ln \beta = 5.5 \quad . \quad [2.71]$$

Equations 2.70 and 2.71 combined, make up one of the three equations that are known as the “law of the wall”(Schlichting, 1979, p. 605). The three equations or curves making up the law of the wall are

$$\frac{u}{u_*} = \frac{zu_*}{\nu} \quad \text{for the viscous sublayer } \frac{zu_*}{\nu} \leq 5 \quad , \quad [2.72]$$

$$^1 \text{Reichardt's curve for the transition layer } 5 < \frac{zu_*}{\nu} < 70 \quad , \text{ and} \quad [2.73]$$

$$\frac{u}{u_*} = \frac{1}{\kappa} \ln \frac{zu_*}{\nu} + 5.5 \quad \text{for fully turbulent flow with } \frac{zu_*}{\nu} > 70 \quad . \quad [2.74]$$

Customarily, the law of the wall is always discussed in association with smooth boundaries as that is the regime where the experiments to validate this law were performed. However, it also has been found that the log law is valid for rough boundaries (Schlichting, 1979, p. 618). From experiments, the distance from the boundary has been scaled with the roughness height, k_s .

Therefore, equation 2.66 now has the form

$$\frac{u}{u_*} = \frac{1}{\kappa} \ln \frac{z}{k_s} + B \left(\frac{u_* k_s}{\nu} \right) \quad . \quad [2.75]$$

¹ (see Schlichting (1979, figure 20.4, p. 601)

The value of B has been determined to vary with the roughness Reynolds number, $(\frac{u_* k_s}{\nu})$, from the work of Nikuradse (Schlichting, 1979, p. 620). However, for a fully rough channel, B becomes a constant value of 8.5, which allows the following log-law equation for a fully rough flow as

$$\frac{u}{u_*} = \frac{1}{\kappa} \ln \frac{z}{k_s} + 8.5 \quad . \quad [2.76]$$

Nezu and Nakagawa (1993) contend that these log-law type equations only are valid in the wall region ($z/H < 0.2$), primarily because the farther away from the boundary, the more invalid the assumption of Prandtl's derivation (constant stress assumption). This result is in contrast to the recommendations of Keulegan (1938) whose work in open-channel flows found that the log law could be applied for the entire depth of flow.

2.2.2.3 Velocity-Defect Law

Velocity equations for the outer region exist that are independent of the boundary roughness (they are valid for either smooth or rough flow). These equations are termed velocity-defect law equations and are derived by starting from the log law.

Continuing with the work of Prantl (1925), assuming at $z=H$, $u=U_m$, which are then entered as a boundary condition into equation 2.66 yielding

$$U_m = \frac{u_*}{\kappa} \ln H + C \quad . \quad [2.77]$$

Subtracting equation 2.66 from 2.77 and placing in dimensionless form yields the well-known velocity-defect law form of the velocity equation stated as

$$\frac{U_m - u}{u_*} = -\frac{1}{\kappa} \ln \frac{z}{H} \quad . \quad [2.78]$$

This form of the velocity profile equation has no dependence on the surface roughness, however, the form is dependent on the assumptions inherent in Prandtl's derivation, namely 1) the mixing-length hypothesis, 2) the mixing length scaling with distance from the boundary, and 3) the constant value of shear stress (equal to the boundary shear stress). The third assumption may be the most difficult to adhere to (although, mentioned previously, results have shown the assumption to be reasonable). Equations that alleviate these assumptions, either by derivation under different assumptions or from additional terms in the equation, are discussed in the following paragraphs.

Von Karman (1931) introduced a similarity rule that assumed that the turbulent fluctuations are similar at all points in the flow field and scale by time- and length-scale factors. Using an empirical constant, κ , he arrived at the equation for the mixing length as

$$l = \kappa \left| \frac{du/dz}{d^2u/dz^2} \right| . \quad [2.79]$$

Substitution of equation 2.79 into equation 2.63 yields the expression for the turbulent shear stress as

$$\tau_t = \rho \kappa^2 \frac{(du/dz)^4}{(d^2u/dz^2)^2} . \quad [2.80]$$

Assuming that the shear stress is linear function of the depth of the channel yields

$$\tau_t = \tau_0 \frac{y}{H} . \quad [2.81]$$

Noting that y is the distance from the water surface and that Von Karman does not make the same assumption of Prandtl, that is that the shear stress is constant and equal to the bed shear stress, applying equation 2.80 to 2.81 yields

$$\frac{\tau_0 y}{\rho H} = \kappa^2 \left| \frac{(du/dz)^2}{d^2u/dz^2} \right|^2 . \quad [2.82]$$

According to Schlichting (1979, p 586), by integrating twice and determining the constant of integration from the boundary condition $u=U_m$ at $y=0$, we get the following non-dimensional velocity-defect equation

$$\frac{U_m - u(y)}{u_*} = -\frac{1}{\kappa} \left\{ \ln \left[1 - \sqrt{\frac{y}{H}} \right] + \sqrt{\frac{y}{H}} \right\} . \quad [2.83]$$

If instead of referencing τ_t to y , measured from the water surface, τ_t is referenced to z , measured from the boundary (as is customary in most applications), equation 2.83 becomes

$$\frac{U_m - u(z)}{u_*} = -\frac{1}{\kappa} \left\{ \ln \left(1 - \sqrt{\frac{H-z}{H}} \right) + \sqrt{\frac{H-z}{H}} \right\} . \quad [2.84]$$

This gives a velocity equation for the outer region that is independent of the constant stress assumption of Prandtl.

2.2.2.4 Wake Function

The log law only accounts for the wall shear stress. This is demonstrated by examining the boundary layer approximations in an order of magnitude analysis. The momentum equation in the x direction can be simplified and written as

$$u \frac{\partial u}{\partial x} + w \frac{\partial u}{\partial z} = -\frac{1}{\rho} \frac{\partial p}{\partial x} + gS_0 - \frac{\overline{\partial u'w'}}{\partial z}, \quad [2.85]$$

where S_0 is the bed slope; p is the pressure; $-\overline{u'w'}$, when multiplied by the density, ρ , is the Reynolds Stress (or turbulent stress) described in equation 2.63; and $u \frac{\partial u}{\partial x} + w \frac{\partial u}{\partial z}$ are the inertial terms. In the development of the log-law, the inertial and pressure forces were, in most part, unaccounted for in the derivation of equation 2.76 (recalling that Prandtl used only the relation between the turbulent shear stress and the velocity gradient). This non-accounting of the forces is evidenced further from observed data in the outer region of the flow, where deviations from the log law and the velocity defect law are noted. Nezu and Nakagawa (1993), calling it the “log-wake law”, add a wake function to the standard log law (equation 2.74) as

$$\frac{u}{u_*} = \frac{1}{\kappa} \ln\left(\frac{u_* z}{\nu}\right) + A + w\left(\frac{z}{H}\right), \quad [2.86]$$

where A is the constant for the typical logarithmic velocity profile ($A=5.5$ in smooth cases) and $w(z/H)$ is a wake function from Coles (1956) in the form

$$w\left(\frac{z}{H}\right) = \frac{2W_0}{\kappa} \sin^2\left(\frac{\pi}{2} \frac{z}{H}\right), \quad [2.87]$$

where W_0 is the Coles' wake parameter, expressing the strength of the wake function.

Equation 2.86 can be placed in velocity defect form as (where U_m occurs at $z=H$)

$$\frac{U_m - u}{u_*} = \left[-\left\{ \frac{1}{\kappa} \ln\left(\frac{z}{H}\right) \right\} + \frac{2W_0}{\kappa} \right] - \frac{2W_0}{\kappa} \sin^2\left(\frac{\pi z}{2H}\right) . \quad [2.88]$$

Equation 2.86 also can be expressed through trigonometric substitution as

$$\frac{U_m - u}{u_*} = -\frac{1}{\kappa} \ln\left(\frac{z}{H}\right) + \frac{2W_0}{\kappa} \cos^2\left(\frac{\pi z}{2H}\right) . \quad [2.89]$$

A procedure to compute Coles wake parameter is contained in Julien (1995, p. 103) and repeated here. The wake term vanishes as z approaches 0; therefore, if the semi-log plot is fitted to the lower part of the velocity profile (figure 2.22), the line is projected to $z/H=1$, and the wake term still is assumed to be zero, Coles Wake parameter can be calculated as

$$W_0 = \frac{\kappa}{2} \left[\frac{U_{\max} - u}{u_*} \right]_{\frac{z}{H}=1} . \quad [2.90]$$

Nezu and Rodi (1986), in experiments on flat-bed, fully developed turbulent smooth-bed flows, found W_0 to vary from 0 to 0.253, with a mean value of $W_0 \approx 0.2$. Coleman

(1981) demonstrated that W_0 increases with increasing sediment concentration, with W_0 ranging from 0.191 to 0.861. Lyn (1993) found that for flow over artificial bedforms, W_0 ranged from -0.05 to 0.1 , while a couple of Delft Laboratory experiments reported values of $W_0 = -0.3$. Lyn stated that these strongly negative values of W_0 are the result of stronger favorable pressure gradients. Lyn (1993) found favorable results in replicating the measured velocity profiles over the bedforms with the log-wake law.

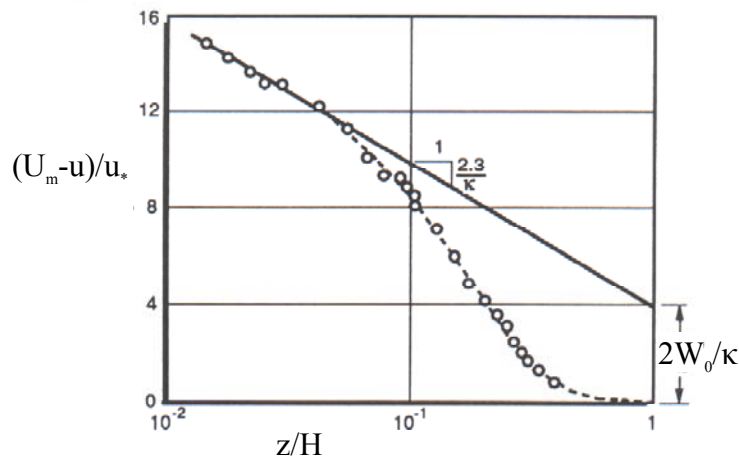


Figure 2.22-Evaluation of W_0 from the velocity defect law (from Julien, 1995)

2.2.2.5 Other Alternative Velocity Models

Other empirical equations that described above have been proposed to describe the departure from the log law (Sarma and others, 1983; Coleman and Alonso, 1983; Song and Graf, 1996); however, these equations are not as widely accepted as the work by Coles (Nezu and Nakagawa, 1993).

Alternative models to the log law for velocity distribution have been cited in the literature. A generalized power law equation was presented by Chen (1991) as

$$\frac{u}{u_*} = a \left(\frac{z}{z'} \right)^m, \quad [2.91]$$

where z' is the physical location of the boundary layer at which $u = 0$, and a and m are a coefficient and an exponent, respectively. Chen (1991), based on theoretical considerations, shows that for perfect agreement between the log law and the power law, the exponent m multiplied by the coefficient a should equal 0.92. Gonzalez and others (1996) found that based on measurements in the Chicago Sanitary and Ship Canal, m was approximately 1/6 and a varied between 4.88 and 5.17.

Swamee (1993) presented a new velocity relation that merges the linear law in the viscous sublayer ($\frac{u}{u_*} = \frac{zu_*}{\nu}$), occurring only for smooth flow, and the log law, occurring for either smooth or rough flow, into one generalized equation for the inner region as

$$u = u_* \left\{ \left(\frac{\nu}{u_* z} \right)^{10/3} + \left[\kappa^{-1} \ln \left(1 + \frac{9u_* z}{\nu + 0.3u_* k_s} \right) \right]^{-10/3} \right\}^{-0.3}. \quad [2.92]$$

2.2.2.6 Added Complexity for Sand-Bed Rivers

For the most part, the preceding discussion essentially has been aimed at clear-water, plane-bed (or flat-bed) flows. When a supply of sediment is available to a river system,

the river has the potential to both move the sediment into suspension and deform the boundary resulting in bedforms.

Various investigators have noted an effect on the velocity profile when sediment was suspended in the flow. Coleman (1981) noted that the amount of the flow represented by the log law shrank as the sediment concentration increased. Muste and Patel (1997) found that the mean velocity, when compared to an equivalent flow, decreased throughout the flow depth as the suspended-sediment increased. Coleman (1981) and Zippe and Graf (1983) emphasized that the log law only was valid strictly in the wall region and that deviations from the log law in these regions should not be accounted for by adjustment of κ and the constant of integration, but rather through application of the wake function. Prior to this finding, experimental studies by many investigators (Vanoni, 1946; Einstein and Chien, 1955; and Elata and Ippen, 1961) had led to the conclusion that κ decreases with increasing suspended-sediment concentration. Coleman (1981) found κ to be independent of the sediment concentration and essentially remains constant. Nezu and Rodi (1986) found κ to be a universal constant independent of Froude or Reynolds number and approximately equal to 0.4.

With the added complexities involved when suspended sediment is present in the flow, some investigators have developed more complex models of velocity. Tsai and Tsai (2000) developed a mathematical model to predict both velocity and suspended-sediment concentration distributions in open-channel flow, with two differential equations solved simultaneously to obtain a solution for the velocity profile. Chiu and others (2000)

developed a new velocity model that is a logarithmic profile with a probabilistic component.

Bedforms will occur along the boundary of the channel during certain flow conditions. In plane-bed flows, u_* and k_s are dependent entirely on the grain-roughness elements on the bed. With the occurrence of bedforms, the velocity profile no longer can be characterized in the typical way using the grain-shear velocity and the Nikuradse type roughness height k_s . Even in the presence of bedforms, some investigators (e.g. Nordin and Dempster, 1963) continued to use the log law throughout the flow depth. In this case, k_s is no longer the Nikuradse equivalent grain roughness, but rather some dynamic combination of the grain and form roughness that will vary depending on where along the bedforms the velocity profile is taken or whether it is a spatially averaged velocity profile. Fedele (1998) states that k_s is a “dynamic variable that accounts for the forces being diffused due to the presence of the wall”. This composite roughness length often is designated as k_c .

Van Rijn (1984C) offers the following relation for the composite roughness length in the presence of bedforms as

$$k_c = 3D_{90} + 1.1H_d \left[1 - \exp\left(-\frac{25H_d}{\lambda}\right) \right] . \quad [2.93]$$

Fedele (1998), utilizing a tactic first introduced by Perry and others (1969), uses Brownlie's (1981) variation of the well-known expression obtained from the Nikuradse data (Schlichting, 1979, p. 621) as

$$\frac{1}{\sqrt{f}} - 2 \log \left[\frac{2H}{k_c} \right] = 1.74 \quad [2.94]$$

to compute the composite roughness length, where f is the total friction factor obtained from the water-surface slope (1.74 is used in the Brownlie (1981) equation, whereas 1.68 is used in the Schlichting (1979) equation). Whereas equation 2.94 was developed for the equivalent grain roughness of sand particles and in this use it is being extrapolated to include both grain-roughness length and form-roughness length, the results that Fedele (1998) reports from actual field data are in good agreement with what Perry and others (1969) derived for a velocity-profile equation.

For flows over bedforms, Nelson and Smith (1989B) suggest that because the shape of the velocity profile varies with position along a bedform, a single log velocity law as given by equation 2.76 is inadequate to describe the entire flow depth. Three models that follow this rationale, Smith and McLean (1977), Nelson and Smith (1989A) and Fedele and Garcia (2001), will be presented in detail in chapter 4. Each of these models determines the extent of the various regions of the flow profile along with computing the necessary parameters for each of these regions. Nelson and Smith (1989B) note that near the boundary, a similarity region is present where the local velocity scales with the local

grain shear velocity. In the flow away from the boundary, the local velocity scales with the overall total shear velocity (that is, the shear velocity averaged over a large part of the bedform field). The different scales of superimposed bedforms determine the number of segments required. The respective scaling parameters (u_* and z_0 , note that $z_0 = k_s/30$), for each segment, are solved by matching successive layers and solving for all layers simultaneously. Nelson and others (1993) present a similar concept to that of Smith and McLean (1977); however, they limit the number of segments to 2.

2.3 Previous Field Scale Investigations

Experiments and investigations regarding flow and shear partitions over fully developed bedforms are numerous. Fedele (1998) summarized the most relevant experiments into three types listed below.

1. Fixed-bed experiments (Vittal and others, 1977; Engel and Lau, 1980; Ogink, 1989; Shen and others, 1990; Nelson and others, 1993; and Bennett and Best, 1995)
2. Movable-bed experiments (Yalin, 1964; Guy and others, 1966; Vanoni and Hwang, 1967; Znamenskaya, 1963; Smith and McLean, 1977; Bridge and Best, 1988; and Kostaschuk and Villard, 1996)
3. Mathematical-model tests (Engelund, 1967 and 1977; Wang, 1981; van Rijn, 1982B; Haque and Mahmood, 1985; Klaassen, 1979)

As expressed earlier, there is an obvious lack of field-scale experiments of velocity measurements over bedforms, especially for large river systems, with the only notable detailed field experiments being those of Smith and McLean (1977) and Kostaschuk and Villard (1996). Among the first to make measurements of velocities in a large alluvial river were Humphreys and Abbot (1861). Humphreys and Abbot made various measurements of velocity along the lower Mississippi River. Based on these measurements, they derived an universal flow-resistance equation for large rivers.

Various researchers were interested in simply collecting bathymetric data to examine the nature and extent of bedforms. Carey and Keller (1957), observed and documented the bed configurations in the lower Mississippi River in Louisiana in one of the first applications of acoustic fathometers. They present graphs of the bedforms along the “sailing line” from New Orleans up to the Old River Control Structure. Bedforms of heights up to 9 m height in approximately 30 m of water were noted in the high-water survey conducted during April 1956. Two bedform scales obviously are present, one bedform scale, which Carey and Keller (1957) term “Super Sand Wave System” has length scales of almost 1.6 km in some cases. Superimposed on these waves are large amplitude bedforms with shorter wavelengths on the order of 60 m (figure 2.23). Carey and Keller (1957) conclude that these large-scale irregularities of the bed vary systematically with discharge and are major sources of flow resistance. Peters (1978, as reported in Julien and Klaassen, 1995) documents bathymetric data for the Zaire River. Julien (1992, as discussed in Julien and Klaassen, 1995) compiled data from unpublished bathymetric surveys on various large rivers including Jamuna, Rhine, and Waal Rivers in The Netherlands, Parana River in Argentina, and the Mississippi River. Julien and Klaassen (1995) present hydrographic survey results from the Meuse, Ijssel, Rhine, and Bergsche Maas Rivers in The Netherlands. van Rijn (1984C) discusses bathymetry data collected on the Mississippi River by Lane and Eden (1940).

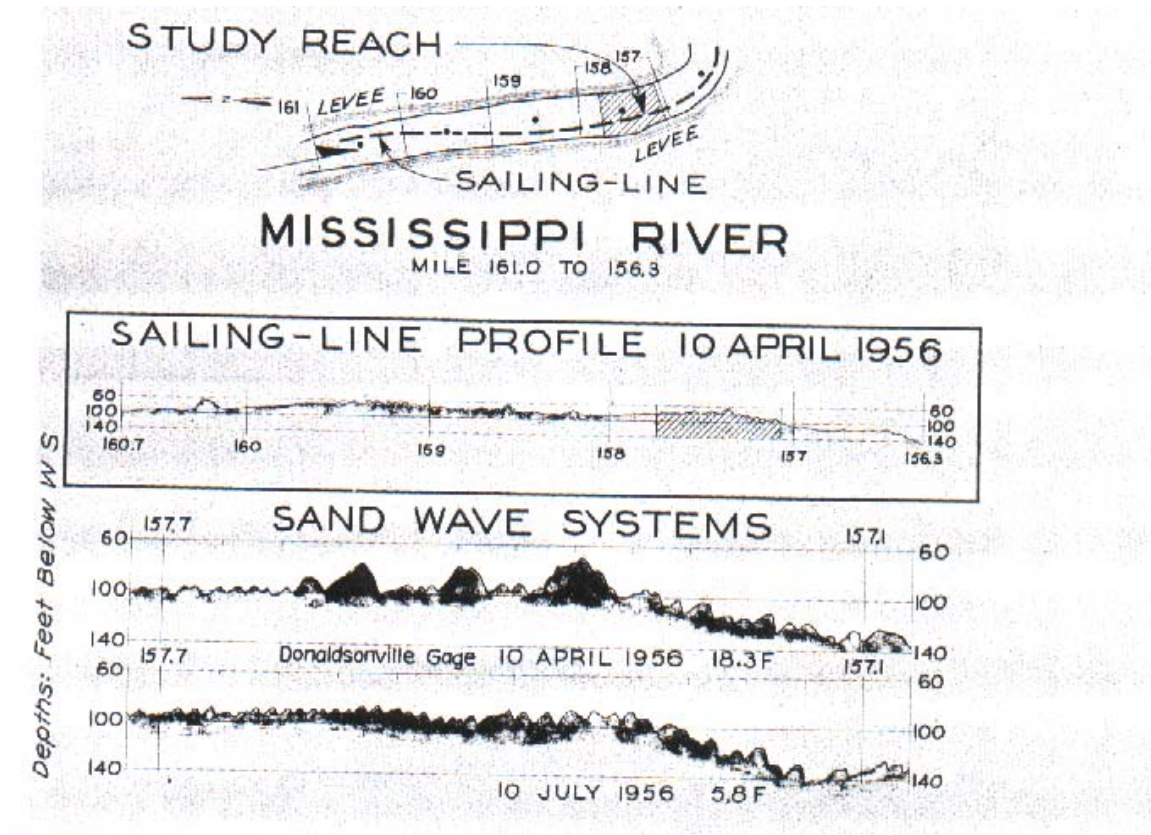


Figure 2.23.—Bathymetric data from the Mississippi River in Louisiana (Carey and Keller, 1957)

The U.S. Geological Survey (USGS), during the late 1940's into the 1950's, undertook several field studies on rivers in the Rio Grande and Missouri River Basins. These studies took on similar characteristics, with the following types of data collection: point observations of velocity with a Price AA current meter, point observations of suspended-sediment concentration using US P46 or modified US DH-48 point samplers, bed-material samples collected and analyzed for size distribution, and salient hydraulic features, including water-surface slope and channel geometry, water temperature, and water discharge.

The Niobrara River near Cody, Nebraska (Colby and Hembree, 1955) was studied as part of a program of the Department of the Interior, Bureau of Reclamation for development of the Missouri River Basin. Data were collected from 1948 until 1953. One of the more interesting features of this study was that in one small reach, all the sediment load being transported was in the form of suspended load. Colby and Hembree (1955) used this site to investigate sediment transport relations, including making a modification to the Einstein (1950) procedure (also see Colby and Hubbell, 1961). No effort regarding defining the bathymetry for identification of bedforms was reported.

The Middle Loup River at Dunning, Nebraska study (Hubbell and Matejka, 1959) collected bedform data with an acoustic transducer. Various other sediment and hydraulic information were collected during the study. Of particular interest was the variation of bedforms with seasons for the same water discharge. In winter, a general absence of bedforms was reported with uncommonly low Manning's n values (Hubbell and others, 1956). Bedform heights ranged from 0.15 to .3 m, with bedform wavelengths ranging from 3 to 5 m.

In the Rio Grande Basin, a large effort (various studies) was undertaken by the USGS to investigate sediment transport, velocity profiles, and bedforms. Several different episodes of data collection took place along the Rio Grande and tributaries with some of the data collected as late as 1969. In the earlier phases (1952, 1958, 1961 data sets) of the studies (Nordin and Dempster, 1963; Culbertson and Dawdy, 1964), channel

bathymetry was not determined rigorously, however, general features of the bedforms were determined (Nordin, 1964). In later data sets (1965-1969) (Culbertson and others, 1972), detailed bathymetric data were collected with an acoustic transducer. Bedform heights ranged from 0.3 to 0.91 m with bedform wavelengths ranging from 6 to 12.2 m. Velocity data were collected simultaneously in the later data sets, using a string of Price AA current meters. The bottom current meter varied from 0.06 to 0.12 m above the bed, in flow depths ranging from 0.73 to 1.4 m.

Jordan (1965) documents various detailed observations of velocity, suspended-sediment concentration, and bed-material size distribution collected on the Mississippi River at St. Louis at the MacArthur Bridge (river mile 178.9). Data were collected at various times from 1948 to 1960. Using bathymetric data obtained from the U.S. Army Corps of Engineers, Jordan reported bedform heights ranging from 0.6 to 2.5 m with wavelengths of on average 76 m in water depths of between 7.6 and 15 m. Bedform wavelengths on the east side of the channel (Illinois side) were observed to be as large as 274 m. Water temperatures also were measured during the study, and as observed in Colby and Scott (1965, p 14), Manning's n did not vary with temperature, although it differed with discharge. Additional data were collected from 1961 to 1963 and reported in Scott and Stephens (1966), including bathymetry data collected by acoustic Fathometer from river mile 174 to river mile 181.

McQuivey (1973A, 1973B) used hot-film anemometry for turbulence, Price AA and Ott current meters for mean point velocity, and various samplers to collect point suspended-

sediment concentrations on the following rivers: Atrisco Feeder Canal to the Rio Grande near Bernalillo, New Mexico; Rio Grande Conveyance Channel near Bernardo, New Mexico; the Missouri River near Omaha, Nebraska; and the Mississippi River near Vicksburg, Mississippi. Data also were collected using various flumes and for the Columbia River estuary near Astoria, Oregon. The velocity and turbulence data were collected for the entire vertical with the exception of near the bed (data collected for the top 90% of the flow depth) Detailed bathymetry data were collected only on the Missouri River. The overall purpose of the study was to correlate turbulence characteristics with hydraulic parameters and suspended-sediment data to gain insight into the flow mechanics.

Smith and McLean (1977) conducted experiments whereby they collected measurements on the Columbia River of velocity and sediment-concentration profiles over bedforms as well as channel bathymetry and bed-material samples (for sediment-size analysis). In these experiments, velocity was measured at four locations in the boundary layer (which this author is interpreting to mean the near-bed region as opposed to the entire flow depth) by use of 4-cm diameter mechanical current meters attached to the frame that Smith and McLean lowered to the near bed. Other observations of velocity were made with a suspended device. They moved the frame 3 meters downstream every hour. Although little detail is provided, the authors state that suspended-sediment samples were collected from a number of stations. The discharge during the experiments ranged from 8000 m³/sec (282,000 cfs) to 17,000 m³/sec (600,000 cfs) with velocities 1 meter from the bed ranging from 50 cm/sec (1.64 ft/sec) to 82 cm/sec (2.69 ft/sec). In the early

experiments (1968 and 1969), the sediment was transported only as bedload, whereas sediment was transported as both suspended-sediment load and bedload during the 1971 and 1972 experiments. In the experiments with only bedload, the bedforms were shorter and steeper than those for the experiments where suspended-sediment load also occurred. These elongated, more symmetrical bedforms induced unseparated flow in the lee of the bedform. Velocity data were collected at time scales such that in examining velocity profiles, they averaged the velocity data over 30 minutes at multiple locations in the vertical and then averaged in the longitudinal direction (along the bedform). They also normalized the velocity data with the velocity measured 1 meter above the bed. (as opposed to normalizing with the shear velocity). Depths ranged from 13.4 to 16.6 m, with bedforms ranging from 67 to 96 m in length and from 1.34 to 3.21 m in height.

Shen and others (1978) reported on data collected on the Missouri River near Omaha, Nebraska at specific times during 1966, 1967, 1968, 1969, and 1975. Data collected were similar to those of Jordan (1965) and Scott and Stephens (1966), using very similar instrumentation and spatial sampling. Part of the motivation of the Shen and others (1978) study was to examine the effects of water temperature on bedforms (and, thus, stage) on the Missouri River. Water temperature was shown to be a definite factor on bedform evolution. For low water temperatures, the bed becomes planar. Shen and others (1978) conclude that the Einstein and Barbarossa (1952) bar-resistance curve agrees reasonably well with observed data on the Missouri River, but does not agree well with data from larger alluvial rivers, such as the Mississippi and Atchafalaya. This conclusion disagrees with that of Jordan (1965), who demonstrated that the bar-resistance

curve agreed well with the Mississippi River at St. Louis data, except at small values of ψ' , where

$$\psi' = \frac{\rho_s - \rho}{\rho} \frac{D}{R_h' S_0} . \quad [2.95]$$

Kostaschuk and Villard (1996) collected flow and sediment data over asymmetric and symmetric bedforms in the Fraser River estuary near Steveston, Canada. Data were collected between May and July 1989 at 4 - 5 verticals along the bedforms. They found no lee-side flow separation for flows over the bedforms; however, this finding may be either the result of inadequate density of flow data or the elongated nature of the bedforms. A Marsh McBirney™ 527 current meter and pump sampler were secured above a 70 kg lead-sounding weight (fish) to collect the necessary velocity and sediment data for this study.